LBL-20310
UC-21

Lawrence Berkeley Laboratory
UNIVERSITY OF CALIFORNIA

Accelerator & Fusion Research Division

RECEIVED
LAWRENCE
BERKELEY LABORATORY
14 1986
ARY AND
SECTION

HEAVY ION FUSION ACCELERATOR RESEARCH (HIFAR)
YEAR-END REPORT: April 1, 1985-September 30, 1985

Heavy Ion Fusion Staff

October 1985

TWO-WEEK LOAN COPY
This is a Library Circulating Copy
which may be borrowed for two weeks.

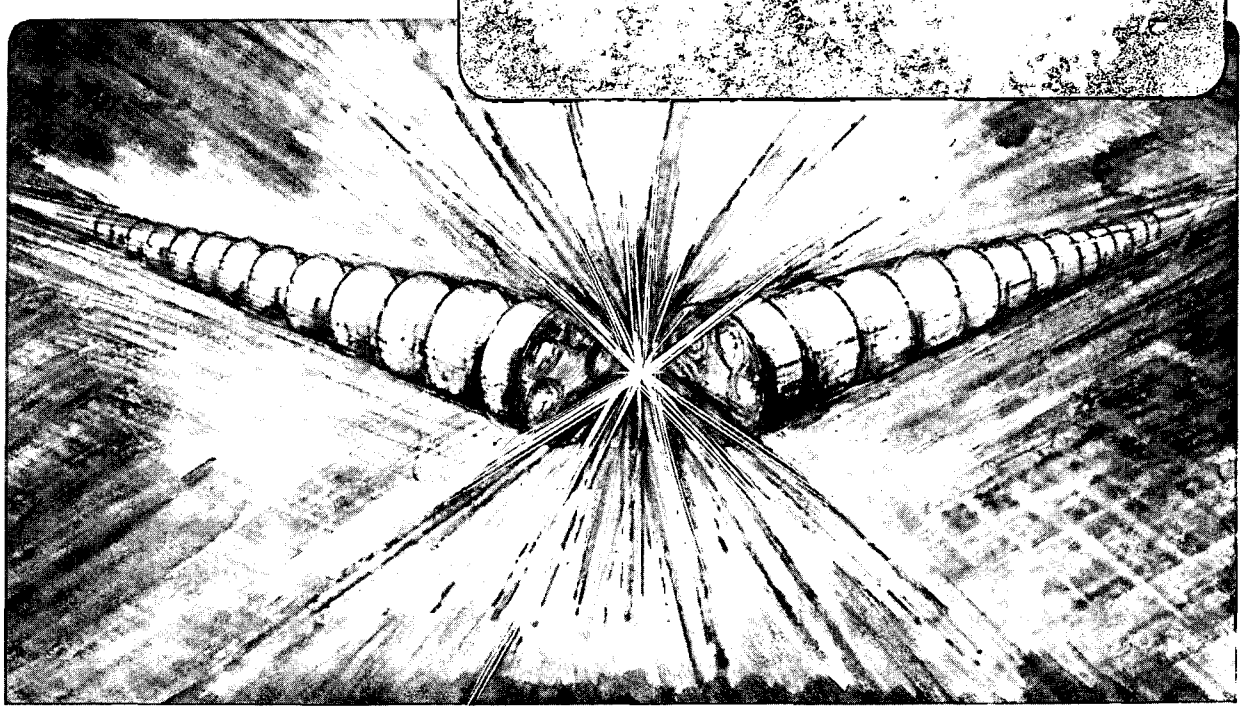

Prepared for the U.S. Department of Energy under Contract DE-AC03-76SF00098

LBL-20310 c.2

DISCLAIMER

This document was prepared as an account of work sponsored by the United States Government. While this document is believed to contain correct information, neither the United States Government nor any agency thereof, nor the Regents of the University of California, nor any of their employees, makes any warranty, express or implied, or assumes any legal responsibility for the accuracy, completeness, or usefulness of any information, apparatus, product, or process disclosed, or represents that its use would not infringe privately owned rights. Reference herein to any specific commercial product, process, or service by its trade name, trademark, manufacturer, or otherwise, does not necessarily constitute or imply its endorsement, recommendation, or favoring by the United States Government or any agency thereof, or the Regents of the University of California. The views and opinions of authors expressed herein do not necessarily state or reflect those of the United States Government or any agency thereof or the Regents of the University of California.

LBL-20310
HIFAN-295

HEAVY ION FUSION ACCELERATOR RESEARCH (HIFAR) YEAR-END REPORT*

April 1, 1985 - September 30, 1985

Heavy Ion Fusion Staff

Accelerator and Fusion Research

Lawrence Berkeley Laboratory
University of California
Berkeley, CA 94720

October 1985

Attention: This document is provided for DOE "Official Use". Distribution to other interested parties is made with the understanding that no information or experimental results given herein will be quoted without first obtaining the authors' permission, or until such information or results have appeared in the open literature.

*This work was supported by the Office of Energy Research, Office of Basic Energy Sciences, U.S. Department of Energy under Contract No.1DE-AC03-76SF00098.

TABLE OF CONTENTS

	Page
HIGHLIGHTS	1
RANGE-ENERGY RELATION FOR HEAVY ION INERTIAL FUSION	4
FIRST ACCELERATION IN MBE-4	5
CURRENT AND KINETIC ENERGY WAVEFORMS FROM THE MBE-4 INJECTOR	6
ENVELOPE CONDITIONING IN THE MBE-4 INJECTOR	7
STATUS OF MBE-4 APPARATUS	8
FOUR-BEAM ELECTROSTATIC QUADRUPOLE DOUBLET ASSEMBLIES	9
INDUCTION CORE ASSEMBLIES	10
MBE-4 ASTRON CORE PULSER MODELS	11
WAVEFORMS FOR LONGITUDINAL DYNAMICS	12
MBE-4 PULSER SYSTEM AND TIMING	13
TRANSVERSE BEAM DYNAMICS	14
ALTERNATIVE CURRENT AMPLIFICATION SCHEDULES IN MBE-4	15
DEVELOPMENT OF COMPUTATIONAL GUIDELINES FOR DESIGN OF MBE-4 ACCELERATION HARDWARE IN SECTION A (GAPS 1-4)	16
REVIEW OF MECHANICAL TOLERANCES FOR MBE-4 ASSEMBLY	17
SINGLE BEAM TRANSPORT EXPERIMENTS	18

Page

A FAST SIMPLE DETECTOR FOR THE HIFAR ENERGY ANALYZER . . 19

PUBLICATIONS AND INTERNAL NOTES 20

H.I.F. STAFF ROSTER 26

DISTRIBUTION LIST 27

HIGHLIGHTS

1. The first four induction acceleration units have been installed in MBE-4, and experiments on accelerating the four beams have begun. These first four units, driven by a total of 8 pulsers, supply roughly triangular accelerating voltages and, on their own, act as a buncher; oscillograms to be seen later show that the beam current is increased and the pulse-length decreased at the end of the bunching section (Section A of MBE-4). Thus the longitudinal emittance ellipses, either as a function of length at constant time, or as a function of time at constant location, are sharply tilted; this tilt has been measured with an energy analyzer. During current amplification in a long accelerator, however, the emittance ellipse at <u>constant time</u> should be essentially untilted. This condition comes about after the addition of further (flat-voltage) accelerating units which will act as longitudinally defocussing lenses that can postpone spatial bunching indefinitely.

2. A variety of acceleration/amplification schedules has been developed, with the beam current rising in proportion to β, β^2 and β^3. In a driver linac with electrostatic quadrupole lenses operating at their voltage-holding limit, the current can be amplified no faster than the first power of β. Typically, such a situation occurs for an ion energy above about 2 MeV. Since MBE-4 will have a top energy of at most 1 MeV this limitation does not apply, and the more aggressive current amplification schedules mentioned can be tested.

3. Engineering tolerances in the fabrication and placement of electrostatic lens arrays has continued to be a subject of great importance as evidenced by several of the contributions in this Report. Alignment errors lead to gradual growth in coherent oscillations of the multiple beams about their axes, which can result in emittance growth for a variety of reasons. Simulation results are reported for

emittance growth in high-current beams (off-axis) in the presence of higher order multipole fields. On the mechanical side, considerable design and fixturing efforts have led to achievement of tolerances of some 0.002 ins. An understanding has been developed of how even tighter tolerances could be held (as desired for a much longer linac) by employing more elaborate coordinate measuring machines not now available at LBL.

4. The electrostatic energy analyzer reported in the previous Half-Year Report (LBL-19501, April 1985) has proved a useful and powerful diagnostic tool as can be seen from results reported below.

5. During this reporting period, an intensive three-pronged attack has taken place on the design problems of the accelerating pulse-power supplies ("pulsers," for short). First, the computer code SLID (by C. Kim) predicts the ideal waveforms required for a particular acceleration schedule; it can also predict how beam behavior will deviate from "ideal" when non-ideal waveforms are applied. Second, pulser experiments in the laboratory enable us to categorize the non-linear impedance behavior of the core packages. Third, circuit analysis leads to specifications for some classes of pulse shapes which can be superposed to provide good approximations to the ideal waveforms. By iteration among these three activities, suitable waveforms for Section A - the bunching section - have been achieved; the design of the downstream pulsers is still under study. Other issues, such as energy efficiency, dynamic range, optimum use of volt-seconds of core, remain as problems for future study.

6. Heckman and coworkers have obtained new results on how rapidly charge-equilibration takes place when low-charge-state gold ions at E/A = 50 MeV/amu enter solid material. The rise in charge-state to the

equilibrium value is found to take place in a few milligrams of material -- somewhat faster than current theory predicts.

7. In May, the HIFAR group presented twelve contributions at the U.S. National Particle Accelerator Conference at Vancouver. Following that, we were heavily involved in the San Diego Workshop on High-Current High-Brightness Injectors, where the experimental results from the Single Beam Transport Experiment and the related theoretical work on transverse beam dynamics were items of considerable interest. On August 5, a HIFAR presentation was made at San Diego, to the NAS panel, chaired by W. Happer, who are charged to report to Congress on the U.S. program in Inertial Fusion.

RANGE-ENERGY RELATION FOR HEAVY ION INERTIAL FUSION

H.R. Bowman, H.H. Heckman, Y.J. Karant, J.O. Rasmussen, A.I. Warwick and Z.Z. Xu*

The objective of Bevalac experiment #730 H is to obtain the range-energy relation for low charge state beams of an ion at energies, $E/A \leqslant 150$ MeV in representative light (CH) and heavy (Au) materials. The experiment addresses problems pertinent to low-charge state beams envisioned for Heavy Ion Fusion (HIF). When such beams penetrate target materials, they will have charges far from their equilibrium values characteristic of their velocity and the target material. As a result, the rate of energy-loss dE/dx of the ions will be low initially, increasing rapidly as valence and outer-shell electrons are stripped from the ions as they approach charge equilibration. Because of the suppressed values of dE/dx for the ions upon penetrating matter, the ranges of the ions in a given material will depend not only on their atomic number, mass and velocity, but also on the charge state of the incident ion. An important aspect of Exp. #730 H is the availability of low-charge-state, high-rigidity beams of heavy nuclei at the Bevalac, where we have utilized Au beams accelerated and extracted at $Z_{accel} = 61$, 35 and 11.

The first phase of the experiment was carried out with Au^{+61} beams at $E/A = 150$ and 50 MeV to obtain the ranges and rates of energy loss rates of Au in high- and low-Z materials under charge-equilibrated conditions. Figure 1 gives the results of our range measurements of Au in CH and Au absorbers, obtained by time-of-flight, integral and differential range measurement technique. The ranges of the Au ions were measured in the energy interval $22 \leqslant E/A \leqslant 152$ MeV using the 152 MeV/nucleon beam (solid points) and in the interval $12 \leqslant E/A \leqslant 50$ MeV using the 50 MeV/nucleon beam (open circles). The R-E data, when fitted to a quadratic polynomial by least-squares, exhibit standard deviations in range R of $\sigma = 0.4\%$, a dispersion that includes all statistical errors attributable to the range and velocity measurements. Included in Fig. 1 are the calculated range-energy relations based on the proton range-energy relation of Barkas and Berger[1] and the heavy ion range data ($E/A < 10$ MeV) of Heckman et al.[2]

During this report period we made measurements on the ranges and energy-loss rates of Au ions, with $Z_{accel} = +11$ and +35 at energies $10 \leqslant E/A \leqslant 50$ MeV, to investigate possible deviations from the R/E relation, Fig. 1, attributable to the low-charge state values of the incident Au ions. The acceleration and extraction of the Au^{+11} at 50 MeV/nucleon for this experiment required the Bevatron to accelerate the ions using the 3rd harmonic, with extraction at 12.2 kG, which was the first demonstration that the Bevatron could be operated in this mode.

Figure 2 presents all of our observations on the dependence of dE/dx for Au beams in a CH absorber having initial charge-states $Z_{accel} = 61$, 35 and 11 in the energy range $40 \leqslant E/A \leqslant 50$ MeV. Denoted as dE/dx(equil) is the dE/dx measured for Au^{+61} ions that have been degraded in energy from 150 MeV/nucleon, thereby insuring charge equilibration. Compared with these data are our dE/dx measurements in CH for beams extracted from the Bevalac at 50 MeV/nucleon with $Z_{accel} = 6$, 35, and 11. These results give evidence that, for the lowest charge-state ions, dE/dx is depressed by a factor about 1/2 relative to dE/dx(equil) after an energy loss $E_{loss} \approx 0.2$ MeV/nucleon has occurred, i.e. after the ions have penetrated about 1.3 mg/cm^2 CH (which includes the thickness of the first scintillator of the TOF system). The measured dE/dx values converge to the equilibrium values by the time the beams have undergone an $E_{loss} \approx 1$ MeV/nucleon, equivalent to a penetration distance of about 3.5 mg/cm^2.

The data are compared with a theoretical estimate derived from the work of Bailey et al.[3] who give dE/dx versus E_{loss} for neutral Au ions at 46 MeV/nucleon in a variety of materials, assuming ion-ion collisions. Although the data can only be compared qualitatively with theory, it is evident that our measurements argue for a shorter equilibration distance (time) than suggested by the theory.

*Fudan University, Shanghai, China

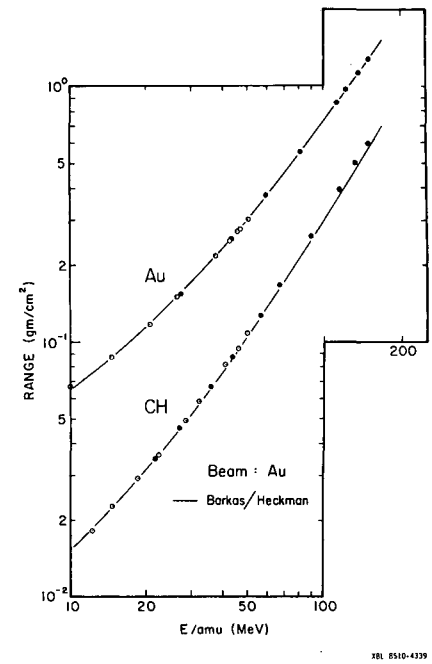

Fig. 1. Range-energy relation for Au ions in CH and Au absorbers. Solid and open circles are data from beam energies 152 and 50 MeV/nucleon, respectively. The curves are predicted ranges from Refs. 1 and 2.

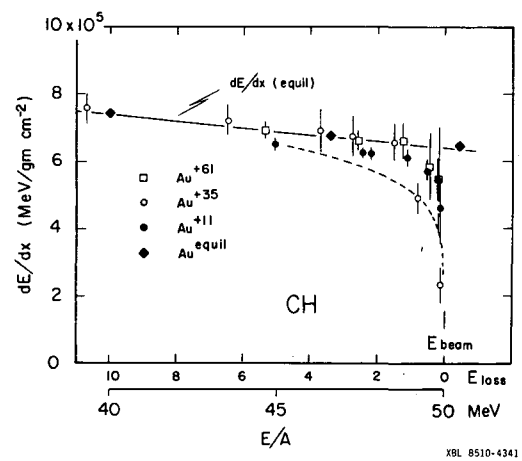

Fig. 2. Energy-loss rates for Au ions in CH for beams at $E/A = 50$ MeV, having charge states $Z_{accel} = 61$, 35 and 11. The data denoted dE/dx(equil) is the observed energy loss rate for ions degraded from $E_{beam} = 152$ MeV/nucleon (see Fig. 1). The dashed curve is derived from the work of Bailey et al.[3]

References

1. W.H. Barkas and M.J. Berger, NAS-NRC Publication 1133, 103 (1964).

2. H.H. Heckman, B.L. Perkins, W.B. Simon, F.M. Smith and W.H. Barkas, Phys. Rev., 117, 544 (1960).

3. D.S. Bailey, Y.T. Lee and R.M. More, Proceedings of the Second International Workshop on Atomic Physics for Ion Fusion, Chilton, Oxon, United Kingdom, Sept. 11-14, 1984.

A. I. Warwick, C. H. Kim and T. J. Fessenden

Following the successful operation of the first eight core pulsers, four cesium beams were injected and accelerated in MBE-4 during the last week of FY 85. Acceleration was achieved using two pulsers on each of the four accelerating gaps of Section A, giving ramped voltage waveforms according to the nominal accelerating schedule.(1) No attempt was made at detailed optimization of the accelerating waveforms at this stage, in fact the nominal schedule is designed assuming uniform current and kinetic energy as initial conditions; these are not realized in the accelerator.(2)

The accelerating voltage waveforms rise from zero at the beginning of the pulse, thus the head retains its original velocity while the rest of the bunch is accelerated in such a way that the current is amplified but remains approximately constant as a function of time, at a fixed location in the accelerator. Figure 1 shows oscilloscope traces of current of the four 5 mA beams measured as a function of time in a Faraday cup array at diagnostic station 5, one period downstream of the fourth accelerating gap. The lower value of current is observed without acceleration; with the pulsers operating, the tail of the beam arrives about 250 ns sooner and the current is increased by approximately 13%. Total charge is conserved. Similar traces were obtained with the maximum intensity 13 mA beams, in this case however it was necessary to scale the voltage of the transport quadrupoles with the energy of the centre of the bunch to avoid beam loss. Both the 5 mA and 13 mA beams are matched for transport with $\sigma_0 = 60°$ and during acceleration it is desirable to maintain $\sigma_0 = 60°$ for the centre of the bunch to minimize transverse mismatch oscillations.

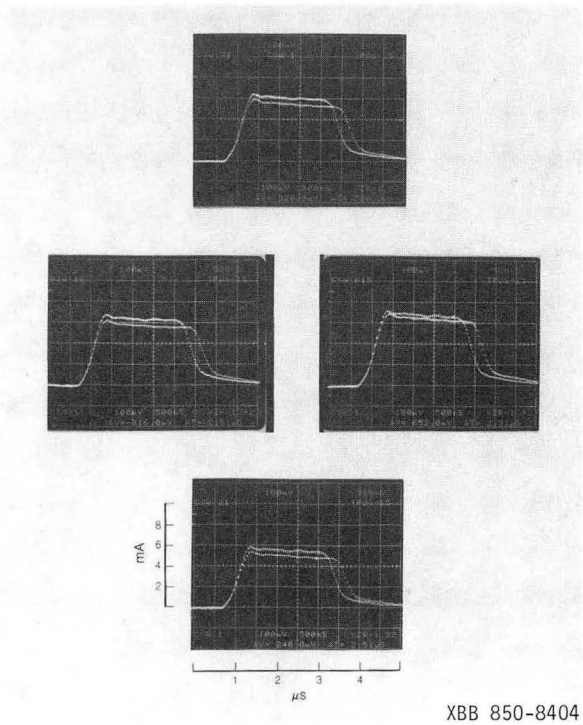

XBB 850-8404

Fig. 1. Current traces of the four 5 mA beams at diagnostic station 5, with and without acceleration.

Figure 2 shows the measured kinetic energy of one of the 13 mA beams with and without acceleration. These data are obtained with our electrostatic energy analyzer over many pulses, changing the analyzer voltage to span the dynamic range. Shot to shot variation of the kinetic energy is less than 0.1%. The data are corrected for the drift time through the instrument, this allows the kinetic energy to be compared to the current measured at diagnostic station 5 (lower part of Fig. 2) as a function of time. The energy rises through the body of the bunch with the tail gaining some 55 keV.

Note that the injector operates in such a way as to give particles with high energy in the leading edge of the bunch and particles with low energy in the trailing edge.(2) The accelerating waveforms used here make no attempt, as yet, to correct this and at diagnostic station 5 the ends of the bunch have begun to drift apart. (Compare Fig. 2 here with Fig. 1 of ref. 2). This is a ballistic effect masking the smaller effects of space charge which are qualitatively the same. Additional pulsers will be deployed in the future to hold the bunch ends together.

Given the actual accelerating waveforms(3) and the measured initial conditions, one can compute the longitudinal behaviour of the bunch.(1) The dotted lines in Fig. 2 show such a calculation of the final energy and current waveforms at this location after acceleration; agreement with the data is excellent.

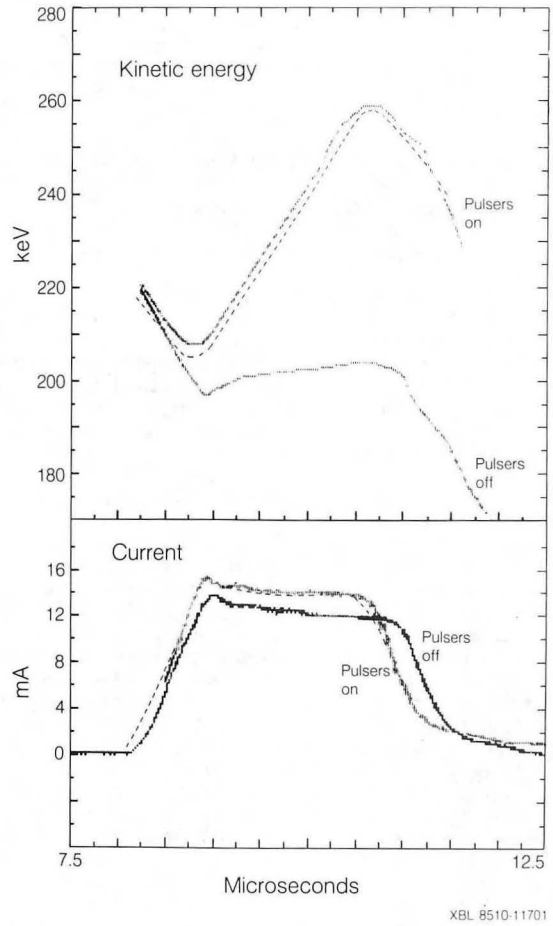

Fig. 2. Measured kinetic energy and current waveforms of one of the 13 mA beams at diagnostic station 5, with and without acceleration. The dotted line is a calculation of the accelerated waveforms for comparison to the data.

References

1. D.L. Judd, private communication
C.H. Kim and L. Smith, Heavy Ion Fusion Half Year Report, June 1985.

2. A.I. Warwick, this report.

3. D.E. Gough, D. Brodzik, and C. Chavis, this report.

CURRENT AND KINETIC ENERGY WAVEFORMS FROM THE MBE-4 INJECTOR

A. I. Warwick

The longitudinal behavior of the beams in MBE-4 is controlled by the schedule of accelerating waveforms,[1] which depends on the initial current and kinetic energy profiles $I(t)$, $T(t)$, before acceleration, at the first accelerating gap.

The MBE-4 injector system, operating in August '85, has produced four matched beams with variable currents of either 5 mA or 13 mA, the latter value being the maximum transmission through the beam conditioning unit. Current and kinetic energy profiles have been measured at the last diagnostic station before accelerator section A, one period upstream of the first accelerating gap.

The time dependence of current and kinetic energy at this point is determined almost entirely by the Marx diode voltage and the space charge in the diode gap. Longitudinal space charge fields have no significant effect over the 2 m transport distance through the conditioning unit. The applied diode voltage is the sum of two pulses, one large pulse (+200 kV) from the Marx itself and a smaller bucking pulse ($\simeq$ -10 kV) used to trim the overshoot of the Marx. In addition to optimizing the timing and amplitude of the trim pulse, the risetime of the Marx was varied, guided by two dimensional time dependent simulations of the diode[2] which showed minimized transient effects at $\simeq$ 400 ns risetime.

Given that the shape of the actual voltage rise was not ideal, parameters were varied to produce the most uniform current waveforms $I(t)$. The corresponding kinetic energy waveforms $T(t)$ showed some time structure, to be corrected by the shaped voltages on the first accelerating gaps.

Figure 1 shows measured current waveforms, for the four beams with nominal 13 mA of current. The time scale is measured relative to the Marx trigger so that it represents flight time from the diodes. These measurements are made in a fourfold array of biased Faraday cups with a time response (based on cup geometry) of about 50 ns. There is some variation of intensity between beams, most noticeably the bottom beam has 10% too little current.

The kinetic energy measurements were made using a 90° electrostatic analyzer,[3] with a secondary emission wire chamber at the focal plane. After verifying that the kinetic energy at this point is a single-valued function of time, by looking at the signals on individual wires, the position of the centroid of the analyzed beamlet was measured as a function of time by coupling the wires resistively and comparing signals at each end of the chain.[4] The time response of this system for these measurements was about 250 ns; faster response is achievable with the sacrifice of signal level. The result for one of the 13 mA beams is shown in Fig. 2. This energy profile is completely measured in a single pulse. The data are extrapolated backwards in time to correct for the transit time through the analyzer and the time scale shown corresponds to that of the current measurements to a precision of ± 200 ns. The head of the beam turns out to have a kinetic energy of about 10% higher than the nominal 200 keV, during the initial part of the pulse when the current is rising from zero and the Marx voltage waveform is climbing like $(1-e^{-t/\tau})$ (τ = 135 ns). There is a minimum kinetic energy about 500 ns into the bunch where the negative Marx trim pulse is at its peak and for long pulses ($\gtrsim$ 10 μs) one observes a slowly falling kinetic energy corresponding to the long-term decay of the Marx voltage.

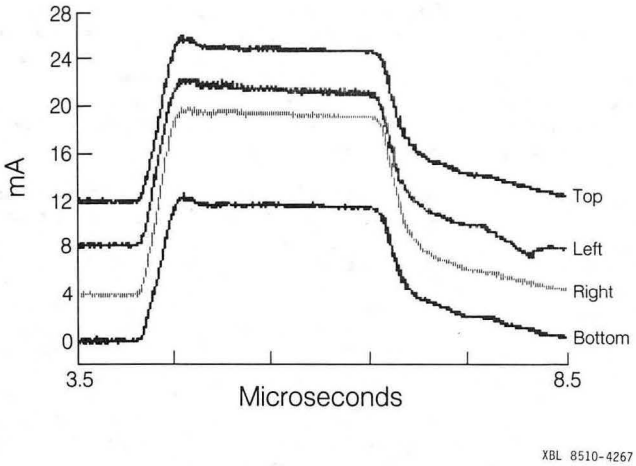

Fig. 1. Current waveforms from the injector, four beams of 13 mA each.

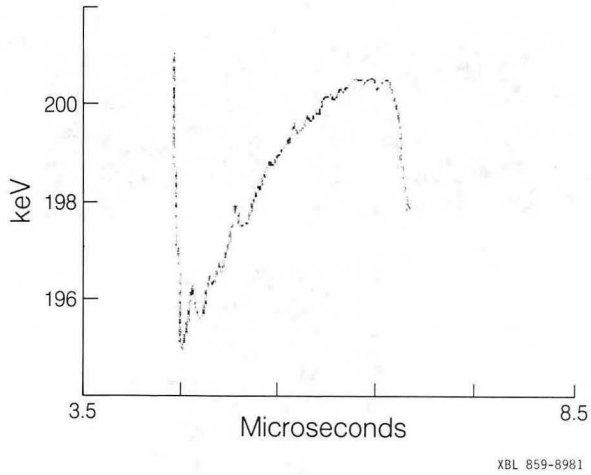

Fig. 2. Kinetic energy versus time for one of the 13 mA beams.

References

1. C.H. Kim and L. Smith, Heavy Ion Fusion Half-Year Report, June 1985.

2. J. Boyd, private communication.

3. S.S. Rosenblum and A. Faltens, Heavy Ion Fusion Half-Year Report, June 1985.

4. T.J. Fessenden, this report.

ENVELOPE CONDITIONING IN THE MBE-4 INJECTOR

A. I. Warwick

The conditioning section of the MBE-4 injector consists of four periods of quadrupole transport between the cesium diodes and the first accelerating gap. By individually tuning the voltages of these eight electrostatic quadrupoles the beam envelope is matched to the periodic solution required in the accelerator.

The problem is underdetermined, there are only four envelope parameters to fit (radii a and b, divergence a' and b'). This allows one to avoid matching solutions which cause the beam to use too much of the aperture. A computer code[1] to integrate the KV envelope equations through the MBE-4 lattice and search for either periodic or matching solutions was implemented as an on-line aid to tuning. Two features particular to MBE-4 were included. The non-linear part of the focussing field[2] was considered in deriving the quadrupole strength from a given electrode voltage and the effect of the changed kinetic energy of a particle on-axis, as it traverses the negative mean potential of the quadrupoles, was approximated by discrete changes in the beam energy and envelope angles at the entrance and exit of the quadrupoles.

The initial conditions for integration of the envelope equations are known only approximately since the measurements at the diode exit were made with partially neutralized beams. Using these approximate values, a K-V calculation gives reasonable voltages for the first doublet and the beams can be transported through it, unneutralized, to the first diagnostic location and carefully measured. Using these results as initial conditions and varying the voltages on four of the quadrupoles a calculated K-V match through the rest of the conditioning section is found, to the periodic KV solution in the accelerator itself. Figure 1 shows such a calculation for a 13 mA beam, note that in this case the aperture of the second doublet is full. This represents the maximum transmittable current at 200 keV.

This calculation gives an initial set of quadrupole voltages for matching which actually produce a beam with envelopes close to those shown. Emittance measuring diagnostics are employed 5 cms upstream of the last symmetry point (a = b) to determine the envelopes. We compare the measured r.m.s. quantities $2\langle x^2\rangle^{1/2}$ and $2\langle x'^2\rangle^{1/2}$ with the calculated matched envelope radius (a) and divergence (a'). The KV calculation yields a response matrix relating changes in the envelope to changes of the quadrupole voltages. Using this relationship the difference between the measured and calculated envelopes can be tuned away by one final iteration (voltage changes of about 15%) to give four beams which are considered matched. Figure 2 shows the result for one of the low current 5 mA beams. The two dimensional histograms are the measured current density versus x and x', y and y', in the horizontal and vertical directions. The ellipses are the calculated shapes of the KV matched beam.

By the means outlined above, the four beams have been matched at two values of current, 5 mA and 13 mA per beam. The match is equally good for all four beams. The 13 mA beams explore most of the aperture (without losing current) and suffer emittance growth as result of the non-linear fields at large radius. The final values of normalized emittance are:

$$\pi\varepsilon_N^{rms} \equiv 4\pi\beta\gamma\left[\langle x^2\rangle\langle x'^2\rangle - \langle xx'\rangle^2\right]^{1/2}$$

$$\pi\varepsilon_N^{rms} = 0.6\times10^{-7}\ \pi\ \text{m rad} \quad (5\ \text{mA})$$

$$\pi\varepsilon_N^{rms} = 1.4\times10^{-7}\ \pi\ \text{m rad} \quad (13\ \text{mA})$$

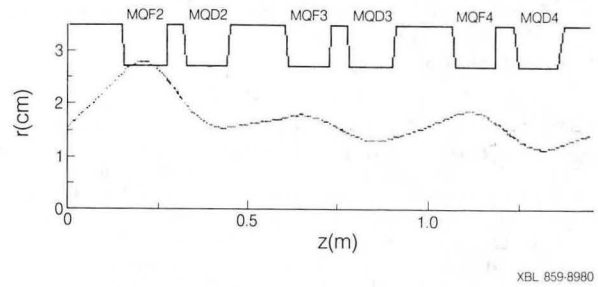

Fig. 1. KV envelopes for a matched 13 mA beam. This calculation shows beam scraping the quadrupoles, but in practice the full current is transmitted.

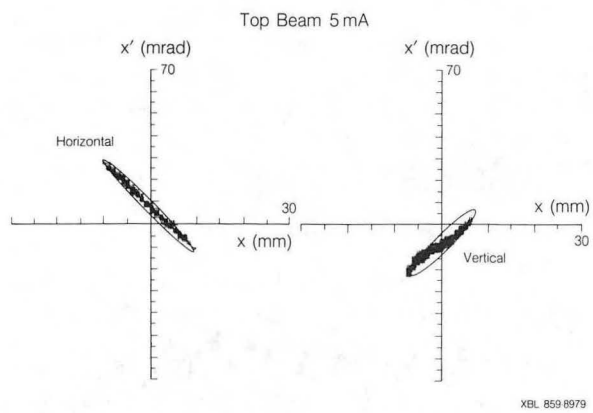

Fig. 2. Measured and calculated phase space distributions for a 5 mA matched beam.

References

1. C.H. Kim, L.J. Laslett, private communication.

2. C. Celata, L.J. Laslett and L. Smith, Heavy Ion Fusion Half Year Report, June 1985.

STATUS OF MBE-4 APPARATUS

R. T. Avery, on behalf of the MBE-4 Team

The apparatus planned for the MBE-4 experiment was described briefly in the last Half Year Report [1] and more extensively in the MBE-4 Program Plan [2]. By the end of March 1985, four cesium ion beams had been transported through cell M0 with the measured performance described in the previous Half Year Report [1].

At the end of September 1985, the MBE-4 experimental apparatus had progressed further to the stage shown diagrammatically in Fig. 1 and photographically in Figs. 2 and 3. The cesium ion beams are now transported through the Beam Conditioning Unit and Accelerator Section "A" to the energy analyzer [1] previously used on the Single Beam Transport Experiment. The apparatus now includes ten electrostatic quadrupole doublet arrays (described in a separate paper in this report) and four induction accelerating gaps (the core arrangement and pulsers for which are described in two other papers herein) plus five diagnostic boxes into which can be placed harps, emittance sensors, capacitance pickup current sensors and Faraday cups for measuring the beam characteristics. The experimental results obtained with this apparatus are reported in still another paper herein.

The entire HIFAR group has contributed to the work described here and their contributions are gratefully acknowledged.

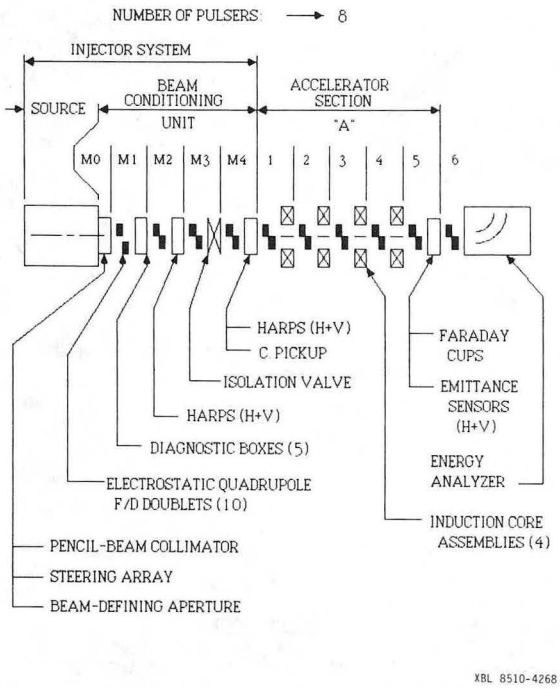

Fig. 1. Diagram illustrating the components installed and operating on the MBE-4 apparatus at the end of September 1985.

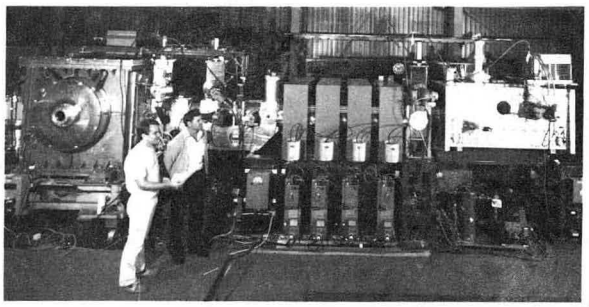

CBB 859-7713

Fig. 2. Photo of the MBE-4 apparatus taken in late September 1985 showing (from left to right): the large tank containing the four-beam source and its pulser; the diagnostic boxes and isolation valve of the Beam Conditioning Unit; the four square housings containing the induction acceleration cores with the induction pulsers located underneath; and finally the large tank containing the energy analyzer. [Photo BBC 859-7713]

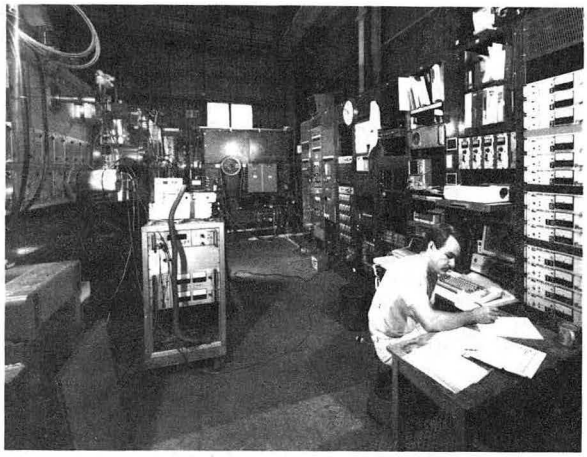

CBB 859-7715

Fig. 3. Photo in late September 1985 showing the MBE-4 accelerating apparatus on the left (with the beam coming towards the viewer), the source pulser in the middle distance and the electronics control, power and diagnostic equipment on the right. [Photo BBC-859-7715]

References

1. Heavy Ion Fusion Half Year Report, Oct. 1, 1984 - Mar. 30, 1985, LBL-19501 (June 1985).

2. R.T. Avery (for HIFAR Group), Program Plan for the MBE-4 Multiple Beam Experiment, LBL-19592 (Feb. 1985). Supercedes PUB-5142.

FOUR-BEAM ELECTROSTATIC QUADRUPOLE DOUBLET ASSEMBLIES

T. Henderson and J. Meneghetti

Fabrication and installation of five Electrostatic Quadrupole Doublet Assemblies for Accelerator Section A of the MBE-4 Experimental Apparatus has been completed. The origin of this experiment and the nature of its goals were discussed in the year end report for FY 1984[1] and further described in the program plan, Feb. 1985.[2] A separate report in this document[3] by R.T. Avery, et al. provides an overview of the present status of the MBE-4 apparatus. Reference to Warwick's report[4] in this document will describe initial beam transport and acceleration results.

An Electrostatic Quadrupole Doublet Assembly is shown in Fig. 1.. Each of these Doublet Assemblies contains 2 Singlet arrays. Each of these Singlet arrays contains 9 electrodes. One Singlet array has 5 electrodes attached to a plate which is electrically grounded while the other four electrodes are attached to a plate which is at negative high voltage. In the other Singlet array this arrangement is reversed with four at ground potential and five at negative high voltage. In each Singlet array ceramic insulators space the high voltage plate from the ground plate. These two Singlet arrays are mounted into a common housing to form the doublet assembly shown in Fig. 1.

Each electrode is 40.23 mm (1.584") diameter and 107.44 mm (4.230") long. The spacing between the centers of the Beamlet Apertures is 66.7 mm (2.625") and the diameter of the aperture is 54.1 mm (2.128"). The outside diameter of the Housing is 322.58 mm (12.700") and the overall length of the assembly is 307.4 mm (12.100").

In order to achieve the precision alignment required for each of the 18 electrodes within a Doublet Assembly, detailed fabrication procedures and fixtures have been developed for each part. Precision fixtures to accurately place each electrode on its electrode plate and to assemble a Ground Array to a High Voltage Array have been fabricated and verified for accuracy using a coordinate measuring machine. A complete description of the individual parts and the assembly fixtures and methods is presented in a separate HIFAR note.[5]

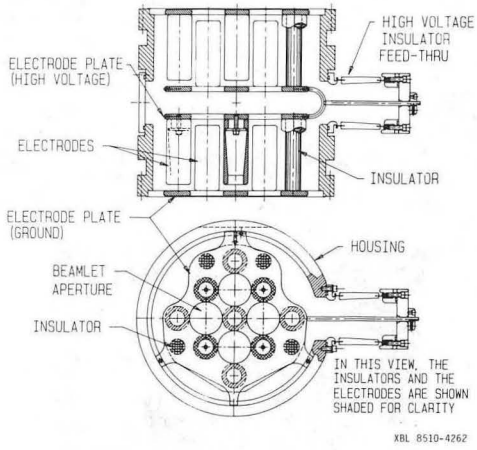

Fig. 1. Four-Beam Electrostatic Doublet Assembly

Measurements taken during and at the completion of these assemblies verify that each electrode in a Doublet Assembly is placed within .002" of "True Position" with respect to the center of the housing.

Figure 2 shows a Single Quadrupole Array about to be installed into a Doublet Housing.

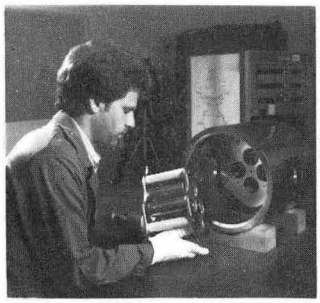

CBB 857-5683

Fig. 2

Figure 3 shows five Quadrupole Doublets assembled with four induction insulators to form the beam focussing assembly for Accelerator Section A, Measurements taken at the completion of this assembly show that each Doublet Assembly is positioned with an accuracy of .0025" RMS. Details of these measurements are described separately.[6]

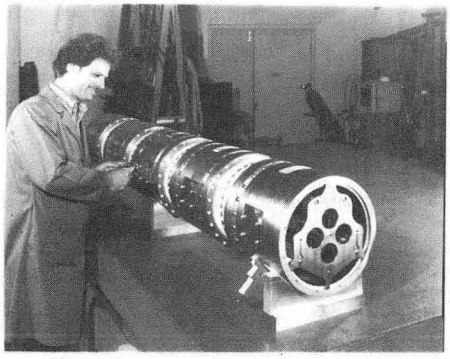

CBB 858-6714

Fig. 3

It is expected that with the precision achieved in this first Accelerator section, a 30 period MBE-4 system will be capable of delivering up to 13 mA Beamlets within the available aperture.

References

1. Heavy Ion Fusion Year-End Report, FY 1984, LBL Report No. 18840 (Dec. 1984).

2. "Program Plan for the MBE-4 Multiple Beam Experiment," LBL Report No. 19592 (Feb. 1985).

3. R.T. Avery, et al., see this report.

4. A.I. Warwick, see this report.

5. "Quadrupole Assembly and Measurements", HIFAR Note 39.

6. "Accelerator Section A - Assembly Measurements", HIFAR Note 34.

INDUCTION CORE ASSEMBLIES

T. Henderson, J. Meneghetti and D. Vanecek

Four core assemblies, one for each of the four accelerating gaps in Accelerator Section A of the MBE-4 experimental apparatus, have been assembled, tested, installed and pulsed to provide the initial acceleration of beams in MBE-4.

This experiment and its goals are fully described in the program plan Feb. 1985.[1] A separate report in this document[2] reports the present status of this experiment. Other reports describe the testing,[3] the induction pulsers,[4] and the initial beam acceleration results.[5] The mechanical packaging of these cores is described here.

The general arrangement of Accelerator Section A is shown in Fig. 1. Each accelerating gap has one core assembly placed around the induction insulator for that gap. Each core assembly consists of 12 Astron[6] cores for a total of 48 cores used in this accelerator section. There are 2 kinds of core packages, one where the primary winding goes around a single core and one where the primary winding goes around three cores. Each assembly contains three single packages and three triple packages (see Fig. 1). Because core packages may be powered individually or jumpered together in any combination, considerable flexibility is provided. The 12 cores in each assembly represent a total of approximately 81 millivolt-seconds per accelerating gap potentially available for acceleration. Since initial acceleration experiments use up to 54 millivolt-seconds per gap, considerable contingency for future experimental needs is provided.

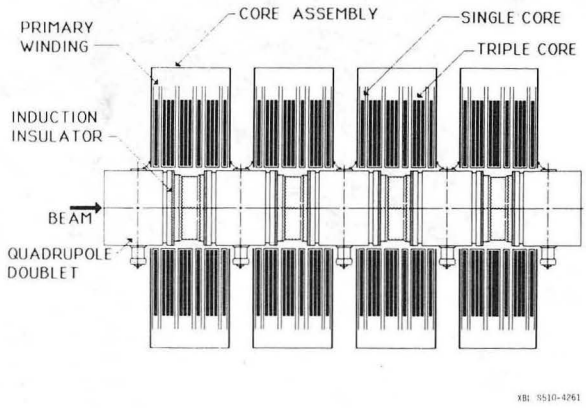

Fig. 1. Accelerator Section A

The Astron cores are wound from .001" thick nickel iron tape. They are 13" I.D., 33.5" O.D. and 1/2" wide. In order to provide adequate space for the induction insulator and the cores primary winding, the I.D. of each core was enlarged to 14". This was accomplished by unwinding the nickel iron tape from the inside diameter. A section taken at the inside diameter of the cores is shown in Fig. 2. The two portions of the primary winding at the faces of the core are made from .020" thick copper sheet. Both of these sheets are cut square so that the corners of the square overlap the O.D. of the core. This overlap area provides a location for electrical connections. The cylindrical portion of the primary, at the I.D. of the core, is .250" thick copper. This cylinder is machined to allow a thin portion of the cylinder to be rolled over to capture the .020" thick sheets. This step in the assembly is shown being performed in Fig. 3. All three parts are pre-tinned with soft solder in the joint area before the cylindrical lip is rolled over. Insulation between the primary and the core consists of 3 layers of .0075" thick mylar sheet at the core faces and the I.D. of the core. The mylar sheets at the faces of the core are cut square and larger than both the primary and the core, see Fig. 3. The joint between each face mylar sheet and each cylindrical layer of mylar at the I.D. is covered with a .0075" thick circular corner cuff of mylar taped in place. The insulation just described between the primary and the core is repeated on the outside surfaces of the primary.

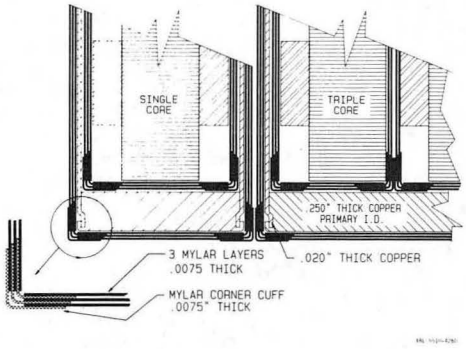

Fig. 2. Core Insulation Details

Fig. 3. LBL Photo #CBB 858-5922

All 12 cores within an assembly are supported at the O.D. by a common wooden cradle. Each core is shimed independently from this cradle so that the inside diameters of all cores are in line. The 12 cores of an assembly, mounted on their common cradle, are enclosed within an aluminum box. The four assemblies required for Accelerator Section A are shown in Fig. 4, the outside covers of the boxes are removed in this photo. The cores are completely enclosed by this box except at the inside diameter of the cores. This aluminum box serves as the secondary circuit and is connected to either side of the induction insulator by flexible wire braid jumpers. These jumpers complete the secondary circuit allowing the accelerating voltage to appear across the induction insulator.

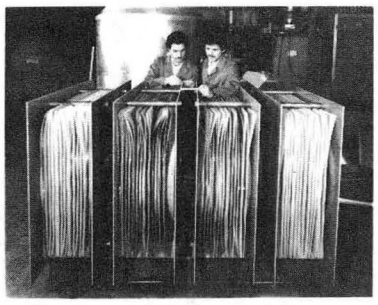

Fig. 4. LBL Photo #CBB 858-6712

References

1. "Program Plan for the MBE-4 Multiple Beam Experiment" LBL Report No. 19592 (Feb 1985).
2. R.T. Avery et al., this report.
3. D. Brodzik, this report.
4. R. Althaus et al., this report.
5. A.I. Warwick, this report.
6. "The Astron Linear Accelerator," IEEE Trans. Nuc. Sci. NS-16, No.3 (1969).

MBE-4 ASTRON CORE PULSER MODELS

D. Brodzik and D. Gough

MBE-4 uses Astron cores in the first acceleration unit and it was necessary to develop a model for these cores. It was found that a pulse line with a characteristic impedance of about 9 ohms was useful in evaluating the core impedance at different voltage levels. It was further found useful to use a series inductance. The pulse line could be modeled as a voltage source with the given characteristic impedance driving the external inductance and the cores (two cores in series were normally used).

Core response (single secondary winding) would then be an initial step which would give information regarding core inductance, rising to a final value determined by the core resistance. It was found that the dominant effect was the core resistance, not the inductance.

One sees, in effect, a core resistance that increases and a core inductance that decreases with an increase in core voltage. A reasonable mathematical model and computer model results if a core resistance of about five ohms/core is used, but no inductance.

Initial requirements for the first accelerator section were to generate two types of core waveforms: parabolic and the so called (1-cos). The (1-cos) consists of a charged capacitor discharging into the cores via a series inductance, with the core paralleled by a second capacitor. The parabolic is achieved by paralleling the core with a resistor instead of a capacitor, the resistance being chosen so that it essentially dominates the node impedance. At first, it was thought that a dominant series inductance driving the core's resistance would result in a core voltage that was of the form $(1-\exp[-t/\tau])$, the expansion of which would approximate a parabolic. This is essentially true, but one always obtained a trajectory with a positive second derivative at low core voltages, the reason being that the increasing core resistance yields a decreasing time constant. At this point, a series of revised accelerating waveforms was obtained based solely on the (1-cos) waveforms (see HIFAR-31). This then immediately led to core and pulser circuit assignment (see HIFAR-32).

Figure 1 and Fig. 2 show the circuit and computer model using the SPICE code[1] for a six Astron core pulser which will be used to generate one of the specified waveforms. The required SPICE predicted and measured waveforms are shown in Fig. 3.

The computer program SPICE was found to be useful in quickly evaluating projected circuits. The version of SPICE used is 2G.6, it was run on a VAX and a compiled version was made available to run on an IBM PC/XT. The only model for the core used was a simple resistor. One might use time dependent switches to model the core's non-linearities, switching in appropriate parallel inductances and resistors. One possibility for the switch would be a diode bridge driven by a pulsed current source. This approach might be used in developing Abramyan type synthesized circuits.

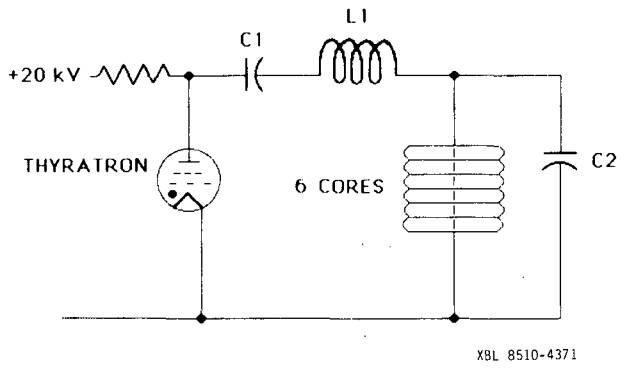

Fig. 1. 6 Core Circuit Diagram

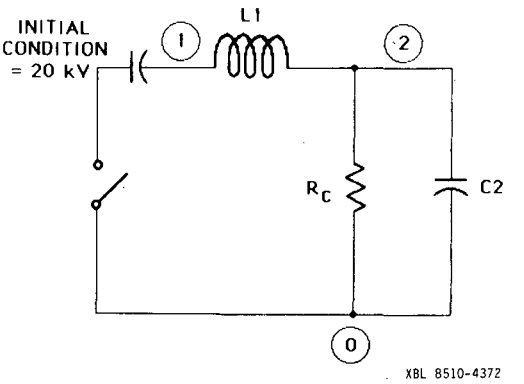

Fig. 2. 6 Core Spice Model

Fig. 3. A SPICE run with actual and desired response is shown below:

```
C1 1 0 .19U IC=22K
L1 1 2 40U
RC 2 0 28.5
C2 2 0 .04U
.WIDTH IN=80 OUT =70
.TRAN .1U 3.5U UIC
.PLOT TRAN V(2)
.END
```

Spice control cards for transient response

legend: * = spice projection
x = actual response
+ = desired response

6 cores x 6.8 milli-vs = 40.8 mvs

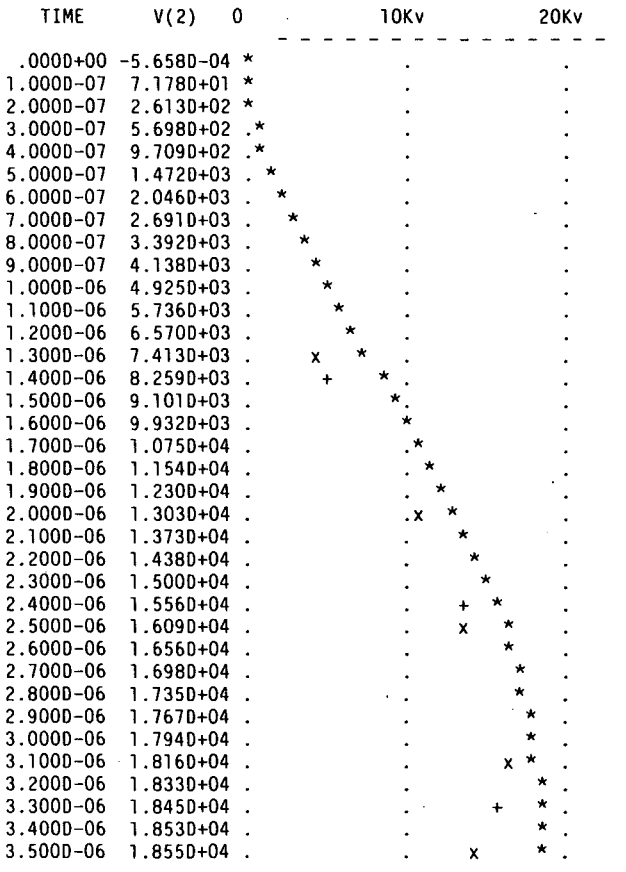

References

1. D.O. Pederson et al., SPICE version 2G.6, University of California, Berkeley.

WAVEFORMS FOR LONGITUDINAL DYNAMICS

L. Jackson Laslett with V.O. Brady

The longitudinal dynamics program SLID[1] for the IBM-PC computer initially was used to synthesize the desired acceleration waveforms through superposition of simple waveforms of two distinctive idealized types, with initial curvatures of opposite sign:

(i) a "one-minus-cosine" waveform, possibly truncated;

(ii) a "parabolic" waveform, possibly clamped.

Use of such waveforms provided useful first estimates of core-size requirements and served to indicate the dynamicsl consequences of imperfect fits or timing errors.

Following such orientational work two new types of waveform were incorporated into the program with the intention that they more realistically would describe the practical performance of actual electrical circuits -- subject, however, to the assumption of linearity in the circuit equations. These circuits are described briefly below and it will be noted that in each case the core impedance has been represented by a pure resistance. Specification of electrical parameters then leads to characteristic time constants for the resulting waveforms (as solutions of a cubic or quartic algebraic equation) and such time constants provide a convenient form of input to the dynamics program SLID. The inverse computation of electrical parameters in terms of the time constants is performed readily by simple arithmetic operations (once the impedance level is specified by assignment of a value to the core resistance) and the results then can be printed.

Modified One-Minus-Cosine Form:

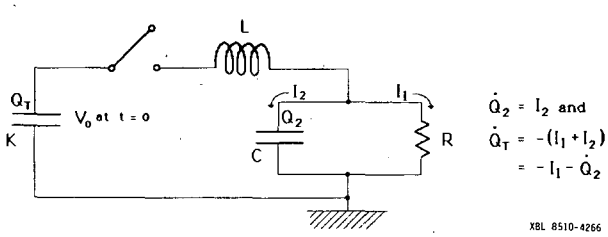

This circuit employs a capacitor in parallel with the core (or resistance R), as illustrated. The electrical response may be written conveniently in terms of roots $[p_1 = -1/\tau_1,\ p_R \pm ip_I = -1/\tau_R \pm i/\tau_I]$ to the cubic equation

$$p^3 + \frac{1}{RC}p^2 + \frac{\frac{1}{C}+\frac{1}{K}}{L}p + \frac{1}{LRCK} = 0$$

as

$$\frac{V(t)}{V_0} = \frac{1}{LC}\,\frac{e^{p_1 t} + e^{p_R t}\left[\frac{p_R - p_1}{p_I}\sin p_I t - \cos p_I t\right]}{(p_R-p_1)^2 + p_I^2}$$

at a time t following closure of the switch. For specified rate factors, p_1 etc., the electrical parameters of the circuit are given by

$$C + K = -\frac{1}{R}\,\frac{p_R^2 + p_I^2 + 2p_1p_R}{p_1\left(p_R^2 + p_I^2\right)},$$

$$C = -\frac{1}{R}\,\frac{1}{2p_R + p_1}, \qquad K = (C+K) - C,$$

$$L = \frac{1}{\left|RCK\ p_1\left(p_R^2 + p_I^2\right)\right|},$$

once the circuit impedance is fixed by specification of R.

Modified Parabolic Form:

This circuit employs as a potential source the rudimentary lumped transmission line illustrated in the diagram shown immediately below. In all applications the internal inductance ℓ shown in series with the core has been taken to be zero, so that the "total" inductance L_T is then given simply by the

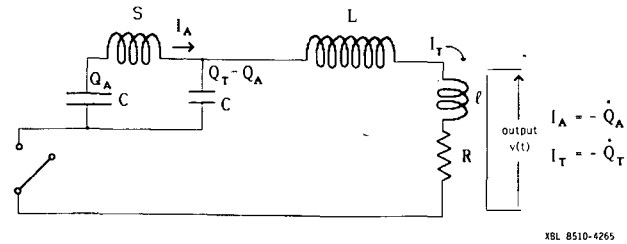

external inductance L. The electrical response is given in terms of roots $[p_1 = -1/\tau_1,\ p_2 = -1/\tau_2,\ p_R \pm ip_I = -1/\tau_R \pm i/\tau_I]$ to the quartic equation

$$p^4 + \frac{R}{L_T}p^3 + \frac{2L_T+S}{L_TSC}p^2 + \frac{2R}{L_TSC}p + \frac{1}{L_TSC^2} = 0$$

as

$$\frac{V(t)}{V_0} = \left(\ell\dddot{y} + R\ddot{y} + \frac{2\ell}{SC}\dot{y} + \frac{2R}{SC}y\right)/L_T,$$

where

$$y(t) = \left[\begin{array}{l} AOF1 \cdot e^{p_1 t} + AOF2 \cdot e^{p_2 t} \\ + e^{p_R t}\left(AOF3 \cdot \cos p_I t + BOF3 \cdot \sin p_I t\right) \end{array}\right]$$

wherein, with

$$D = p_I(p_2-p_1)\left[(p_R-p_1)^2 + p_I^2\right]\left[(p_R-p_2)^2 + p_I^2\right],$$

$$AOF1 = -p_I\left[(p_R-p_2)^2 + p_I^2\right]/D$$

$$AOF2 = p_I\left[(p_R-p_1)^2 + p_I^2\right]/D$$

$$AOF3 = p_I(p_2-p_1)(p_1+p_2-2p_R)/D$$

$$BOF3 = (p_2-p_1)\left[p_R^2 - p_I^2 + p_1p_2 + (p_1+p_2)p_R\right]/D.$$

The solution for the output function V(t) then is readily expressed, as indicated earlier, in terms of these coefficients. With the time constants given, as $\tau_1 = -1/p_1$ etc., moreover, the corresponding electrical parameters are

$$C = -\frac{1}{2R}\,\frac{2p_1p_2p_R + (p_1+p_2)\left(p_R^2 + p_I^2\right)}{p_1p_2\left(p_R^2 + p_I^2\right)}$$

$$L_T = -\frac{R}{2p_R + p_1 + p_2}$$

$$S = \frac{1}{p_1p_2\left(p_R^2 + p_I^2\right)}\,\frac{1}{L_TC^2}$$

in terms of R.

The performance of pulser circuits developed for MBE-4 of course may depart from that described in SLID computations not only because of the restrictions on the size of electrical components available from stock but also, and more importantly, as a consequence of significant non-linearities in the response of circuit elements such as the induction cores. The dynamical consequences of the first of these sources of error of course can be investigated with the program SLID through use of the analyses outlined in the preceding paragraphs, accompanied by compensatory readjustments of the switching times and/or initial potential levels. A computational study of the performance arising from the actual waveforms found to arise from nonlinear elements, however, may require a more elaborate or ingenious modification of the equations.

References

1. C.H. Kim, V.O. Brady, T.J. Fessenden, D.L. Judd, L.J. Laslett, "Synthesis of MBE-4 Waveforms," IEEE Trans. on Nucl. Sci., 32, p. 3190 (1985).

MBE-4 PULSER SYSTEM AND TIMING

R. Althaus, D. Brodzik, C. Chavis, D. Gough

A pulser has been developed to drive the Astron core assemblies. The individual blocks had previously been developed as separate packages, these now have been consolidated into one unit. The time frame for design completion, construction, debug and installation of eight pulsers encompassed about eight weeks.

The pulser is contained in a double box, the inner at soft ground and the outer at hard ground. A +5y trigger (TTL level) is received differentially and applied to the soft ground environment via a fibre optic cable. The received trigger is then processed to result in two trigger functions: an immediate 200 nsec +600V thyratron trigger and a 1 msec delayed 30 μsec wide +5V core reset trigger. The switch function is provided by a hydrogen gas thyratron (English Electric CX1538 or ITT F-227). The circuitry provided for the thyratron of bias voltage, trigger voltage, keep alive voltage and heater voltage is suitable for either of the specified thyratrons. A core reset circuit is used so that the total magnetic flux capability (+B to -B) of the core is realized. Reset is achieved by generating a half sine current pulse of opposite polarity to the normal current pulse, typically 2 msec wide and 300 amps peak. The pulser is designed to operate with an external charging power supply of up to 25 kV. The pulse forming network and high voltage connections are similarly rated.

The first major problem was a voltage oscillation that was determined to be caused by the tube inductance and power supply cable capacitance. It was initiated at tube turn on and could be seen superimposed on the tube's arc drop. A 1 kΩ resistor in series with the charging power supply and an RC snubber at the tube's anode corrected this problem.

Installation of eight pulsers at accelerator section "A" proceeded smoothly and resulted in the predicted gap voltages with the exception of the second gap. The problem seemed to be associated with the first group of three cores. The gap voltage monitor showed, at a fixed voltage level, a brief burst (~ 1 μsec) of higher frequency ringing. The core load arrangement was changed to exclude the suspect group of cores. The problem persisted, but at a higher threshold voltage. These three cores had to then be essentially isolated from the main driving cores by connecting one end to ground. Successful operation of all pulsers followed.

The acceleration voltage across the gap is monitored by a resistor divider and the following waveforms are those obtained for the first four gaps.

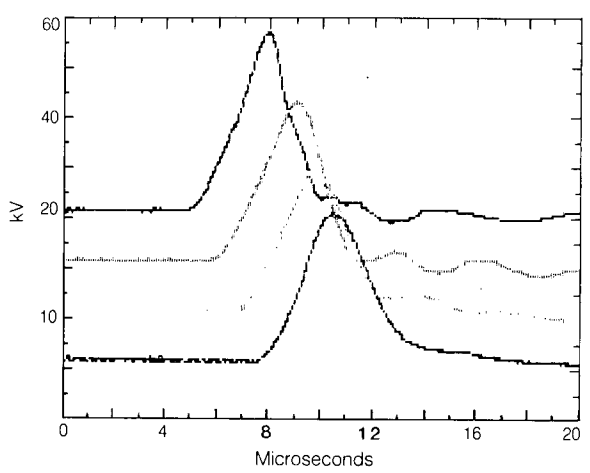

XBL 8510-11703

Fig. 1. Accelerating waveforms in the first four gaps. Time is measured with respect to the Marx trigger and the voltages are shown with offset zero levels.

Timing

A CAMAC timing system was designed to provide the timing requirements for accelerating and shaping the beam. A CAMAC size 2 Timing Control Module was designed to provide start and reset signals for up to 10 ea. 8-Channel Timing Modules. The Control Module provides start control signals at a repetition rate of 0.1 to 1.1 Hz synchronized to the AC line with a variable phase angle. Provision is also made for AC line synchronized external or computer-generated timing system start control signals. The 8-Channel Timing Modules were wire-wrapped in size 2 CAMAC modules using a newly developed CAMAC breadboard (40Y 3201) and IBM-compatible wire-wrap program. Each module has 8 independent delay generators which can be preset manually (via front-panel switches) or by computer (via GPIB Crate-controller and CAMAC crate). The delays are variable from 10 nsec. to 99.99 μsec. in 10 nsec. increments with < 2 nsec. jitter and are displayed on the front panel with miniature 5 digit LEDs. A jumper-plug on the board allows individual selection of either an external "start" or a "start" after another channel delay. Twisted-pair outputs are provided to facilitate noise-immunity on long runs to the triggered equipment.

A typical timing arrangement is shown at Fig. 2. The three Marx triggers and pulser channel number one are shown referenced to the master control. Subsequent pulser channels of the same group are shown referenced to pulser number one.

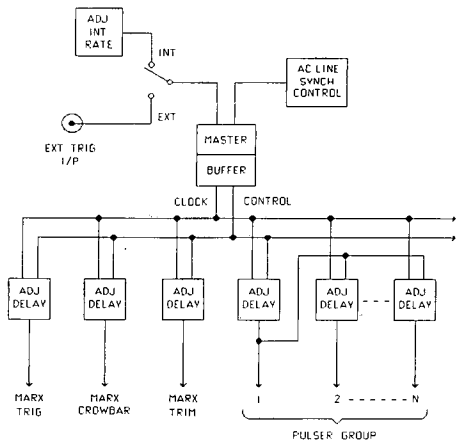

XBL 8510-4370

Fig. 2. Typical Timing Arrangement

C.M. Celata, L.J. Laslett, L. Smith

Investigation of the effect of nonlinear focusing fields on misaligned beams has continued, using the particle-in-cell computer simulation code. In particular, the effects of the dodecapole force which can arise if the ratio of electrode radius to aperture, R/d, is not the "magic ratio", and of the alternating-sign octopole due to the end effects of the quadrupoles ("interdigital nonlinearity") were studied to determine scaling of emittance growth with experimental parameters. Both forces were applied using a thin lens approximation, with strengths chosen using results of the Poisson code for MBE-4 geometry.

The dodecapole causes an oscillation and growth of emittance, with the frequency of the oscillation approximately twice the coherent betatron frequency. The emittance growth was found to be approximately proportional to the amplitude of the oscillation. Both were proportional to the product A_6h, where the nonlinear potential is of the form $A_6(r/d)^6 \cos(6\theta)$, and h is the initial beam centroid offset. The emittance growth increased with increasing σ_0 or decreasing σ. During the emittance growth, a damping of the beam centroid motion was observed. Both the rms beam radii and the particle momenta increased, as shown in Figs. 1 and 2. These phase plots indicated the presence of a mode of even symmetry-- perhaps the $j = 0$, $m = 4$ mode. For low σ/σ_0, this mode has a frequency approximately equal to the coherent betatron frequency, and could be driven by the dodecapole force, which, in the frame of reference of the (oscillating) misaligned beam, has an octopole component. Note that in MBE-4 the effect of the dodecapole should be cancelled by image forces, as explained in the Oct. 1 1984 - March 30, 1985 Heavy Ion Fusion Half Year Report.

The interdigital nonlinearity was found to cause no emittance growth for the nonlinearity strength present in MBE-4. When the strength was greater than double this value, however, an emittance oscillation with accompanying emittance growth was observed for misaligned low σ beams. The oscillation frequency was again twice the coherent betatron frequency, and caused heating of the beam, but no change in beam rms radii. Emittance growth, $\Delta\epsilon/\epsilon$, was proportional to the nonlinearity strength times the misalignment, A_4h, with A_4 defined analogously to A_6 above. The emittance growth increased with decreasing σ/σ_0, as for the dodecapole. Lowering σ/σ_0 causes the frequency of the mode being driven to approach the frequency of the driving force, the coherent betatron frequency, and thus is expected to cause the increase in emittance growth seen in the results mentioned here and in the previous work with image forces. The presence of the interdigital nonlinearity was also observed to increase the amplitude of the beam centroid excursion.

As mentioned above, in MBE-4 the effects of the dodecapole and image forces on the beam are expected to cancel. This has been seen in simulation runs, as detailed in the last half year report. A study has been started to determine the feasibility of separating the dodecapole and quadrupole functions into different focusing units. This would permit separate tuning of the two fields, and also perhaps make construction simpler for the magnetic focusing section of the accelerator. To be economically feasible, the number of dodecapole magnets required should be much less than the number of quadrupoles. A computer study to determine the number of dodecapoles required has begun. Dodecapoles were placed at every third lattice period, and their strength varied to minimize emittance growth. Though emittance growth was decreased from the case with no dodecapoles, and its onset was delayed, this procedure was not successful in suppressing emittance growth. However, the dodecapoles added did not alternate sign, as of course occurs in the structure with combined quadrupole-dodecapole electrostatic focusing studied previously. Further computational work incorporating this feature, and well as analytical work to understand the cancellation of the nonlinear forces, is needed in order to explore the utility of this approach.

Finally, the evolution of a beam with a non-uniform density profile is being studied. Work in progress concerns the changes in the beam emittance and distribution function

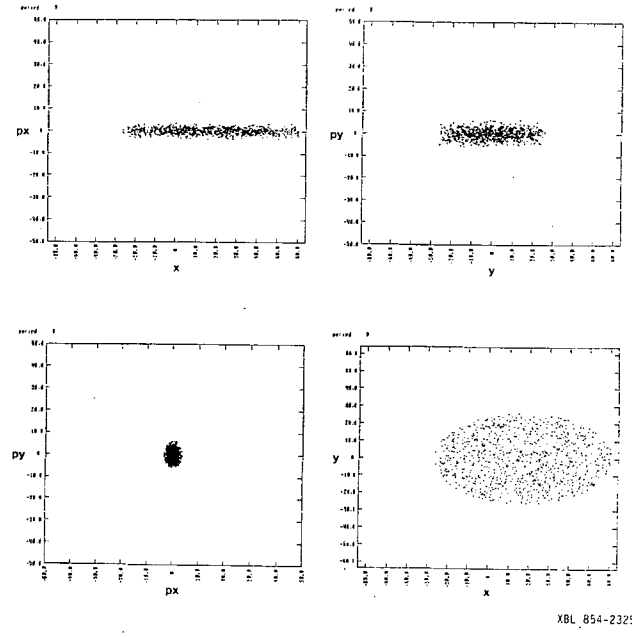

Fig. 1. Phase space, momentum and density plots for beam at the initialization of the simulation. R/d = 0.573, σ_0 = 60°, σ = 6°, a/d = 0.523.

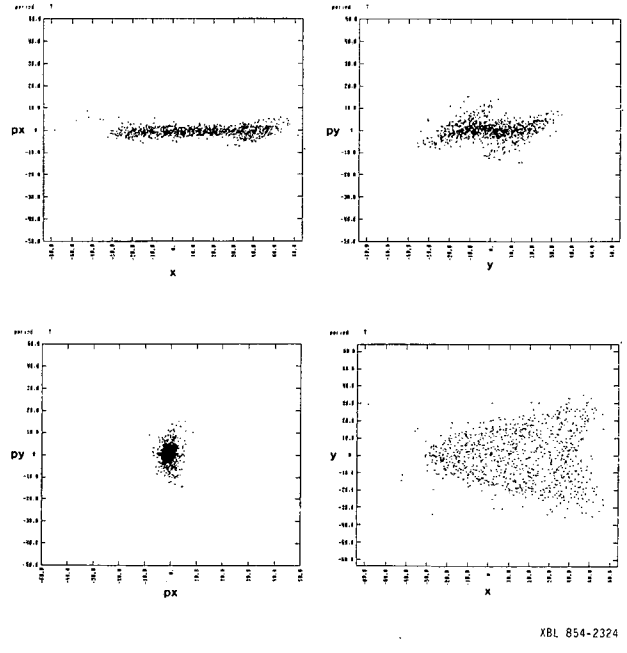

Fig. 2. Phase space momentum, and configuration plots at Period 7 for the parameters of Fig. 1.

(1) during transport through the accelerator, and (2) during its passage through the diode, due to an initial non-uniform spatial distribution. Simulation results show that emittance growth occurs predominantly in the first plasma period, but oscillation of the emittance can persist if the nonuniformities are such as to cause a mismatch oscillation. Comparison with the results of T.P. Wangler ("Relation Between Field Energy and RMS Emittance in Intense Particle Beams," Vancouver PAC, May, 1985, to be published) is in progress. An investigation of the evolution of the beam during space-charge-limited flow in the diode has also been initiated, using a fluid approach.

ALTERNATIVE CURRENT AMPLIFICATION SCHEDULES IN MBE-4

C. H. Kim

Introduction

In the reference design, beam current increased linearly with kinetic energy (E) with a current amplification factor of 4 at the end of MBE-4. In this report, two additional scenarios are presented where beam current (I) increased as ($E^{3/2}$) in one case and as ($E^{1/2}$) in the other. For each case, corresponding accelerating voltage waveforms, required quadrupole voltages along the linac, and the evolution of beam envelopes along the linac for head, center and tail of the bunch were calculated.

In order to keep the beam envelopes matched during the acceleration, the value of σ_0 should be kept constant and, at the same time, beam current should be amplified to the right value after each acceleration gap. Variations from these rules will cause mismatch oscillations which could reduce the transportable current below the theoretical space charge limit. Therefore, any such variation must be attempted in an adiabatic way such that the fractional changes of these variables in one lattice period are small.

Envelope matching can be maintained in MBE-4 by increasing the quadrupole voltages linearly with E and increasing the beam current as $E^{3/2}$. The situation is somewhat different for the front end of HTE where the quadrupole voltage is already at the nominal breakdown limit. In this case, matching can be maintained by increasing the length of quadrupoles as $E^{1/2}$ and amplifying beam current as $E^{1/2}$.

Case A: Current Increases as $E^{3/2}$

A set of accelerating voltage waveforms for case A is shown in Fig. 1. The first 4 "triangular" waveforms and the "square" waveforms are similar to those of the reference design. Two bunching waveforms of "triangular" shape are added at gaps 6 and 7. The head to tail velocity tilt reaches its peak value of 30% right after gap 8. Three debunching waveforms which have voltages decreasing in time are required at gaps 14, 19, and 21 to prevent current from being amplified too much near the end of the linac. Final kinetic energy (780 keV) is smaller than that of the reference design (827 keV) as a consequence of the bunching and debunching operations. These waveforms require about 40% less core material than those of the reference design.

Quadrupole voltages are increased linearly with kinetic energy of the reference particle located at the center of the bunch. For σ_0 = 60° operation, quadrupole voltages increase from 16.5 kV to 66 kV and reaches the present breakdown limit of 50 kV at the beginning of the linac section 'E' (gap no. 26).

The beam radii for the head, center, and tail of the beam were calculated for a 13 mA 200 keV cesium +1 beam. The output current was 100 mA per beamlet. The maximum matched beam radius in the middle of the focusing lens is 18.9 mm (70% of the aperture). Calculation showed mismatch oscillations, probably due to the fact that the current is not exactly amplifying as $E^{3/2}$ as shown in Fig. 2. The maximum radius oscillated between 16 mm and 22 mm.

Case B: Current increases as E

This case is identical to the reference design. Although current is not amplifying as rapidly as in case A, the quadrupole voltages had to be increased linearly with E in order to reduce the mismatch oscillations. The maximum matched beam radius should decrease as $E^{1/2}$, but because of mismatch oscillations the value did not decrease.

Case C: Current Increases as $E^{1/2}$

For the front end of larger induction linacs such as HTE, it is desirable to choose quadrupole voltages close to the breakdown limit and increase I as $E^{1/2}$. The lengths of the lattice-half-period (L) should be increased continuously as $E^{1/2}$, but because of the engineering simplicity, one may want to increase them in discrete steps. In order to simulate this, the quadrupole voltage is fixed and the current is increased as $E^{1/2}$ in MBE-4. We found that the mismatch oscillations became intolerably large after about 8 periods.

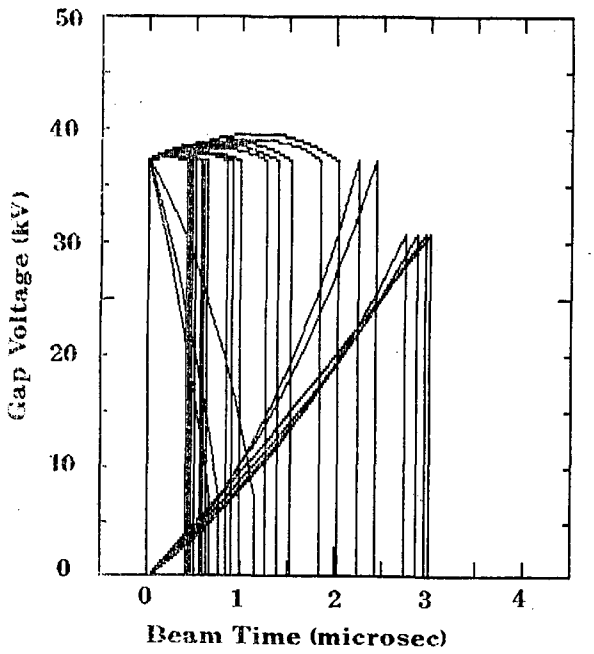

XBL 8510-4269

Fig. 1. A set of accelerating voltage waveforms for MBE-4 which causes beam current to amplify approximately as $E^{3/2}$.

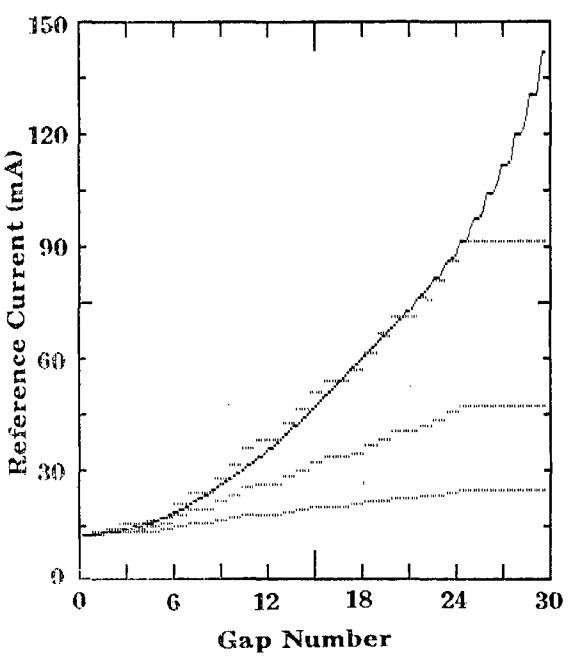

XBL 8510-4270

Fig. 2. Reference beam current versus z (solid line). $E^{1/2}$, E, and $E^{3/2}$ curves are plotted for comparison (dotted lines).

DEVELOPMENT OF COMPUTATIONAL GUIDELINES FOR DESIGN OF MBE-4 ACCELERATION HARDWARE IN SECTION A (GAPS 1-4)

David L. Judd

In this work no "optimized" specifications have been produced; rather, acceptable arrangements have been arrived at by a limited amount of numerical experimentation. The work is based on a particular acceleration schedule* developed[1] by C. Kim, and uses his computer program for longitudinal dynamics. It incorporates his desired behavior as "ideal" and includes longitudinal space-charge effects. It has provisions for introducing non-ideal accelerating waveform components in an interactive mode at every accelerating gap, and for evaluating (to a limited extent) the resulting departures from desired beam bunch behavior. It calculates from an injected beam bunch having constant ion kinetic energy (200 eV); the current is constant during a central time of 2 μs and falls to zero parabolically in 1/2 μs at each end. The level of constant current has mostly been set at 5 mA, but some calculations have been made using 2 mA and 10 mA to test the sensitivity to current.

In the low-current limit the ideal waveforms are determined in a simple way[1] from the acceleration program. These are nearly right triangles at the first four gaps because the bunch head must not be accelerated until the tail is inside the linac, when the head is near to the gap $N = 4$. For finite currents one needs "ears" at bunch head and tail whose strengths depend on current and whose shapes depend on the assumed variations of current at the bunch ends. For the assumed parabolic distributions the ears are approximately linear.

The shapes of waveform components assumed available for fitting have gone through some evolution. At an early stage it seemed obvious that if straight lines were to be approximated by curved components the supply of these should include both concave-upward and convex-upward elements. (Linear rise was regarded as unlikely to be achieved.) The former were exemplified by "one-minus-cosine" shapes and the latter by "parabolic" shapes. In addition, it was assumed that after rising parabolically to horizontal tangency a component could be "clamped" to a constant value. Using these forms, Kim made extensive waveform fitting studies and established approximate but useful properties for MBE-4 out to $N = 30$, such as numbers of pulsers, cores, and volt-seconds needed in the different gaps. After work began on constructing test circuits containing cores it became evident that no shapes were convex upward near their starting times. Further, it was realized that computational waveforms should include only shapes resembling realizable ones. Some simple lumped-element linear circuits were analyzed, and analytical expressions were developed for voltages appearing across elements resembling induction cores. This work[2] resulted in the consideration of two classes of waveforms, called "Laslett modified one-minus-cosine" and "Laslett modified parabola," which have been used almost exclusively in recent computational work. An example of one of these is defined by an applied voltage V_0, a turn-on time T_0, and three, or four, respectively, shape constants which may be specified in time units if desired. Contact with the experimental work on waveform generation is made by selecting shape constants corresponding to achievable types of shapes.

In trying to fit required waveforms in the first gaps it was found that satisfactory fits could be made using only the "modified one-minus-cosine" shapes. Electrical and mechanical design work had progressed to the stage where the maximum number of pulser switches in these four gaps was defined as twelve; accordingly, these fits used a total of twelve components. In addition, it was found possible to make acceptable fits by confining the shapes to only three classes, each defined by three particular values of the shape parameters T_I, T_R, T_I. The first class (a), with one per gap, supplies most of the acceleration and has a high applied voltage (~ 20 kV, taken as the maximum allowable) at each gap. The second class (b) has smaller voltages, in the range 5 to 10 kV, for each of its four elements. The third class (trimmers) has still smaller voltages, about 3 kV or less, and short duration.

It was then determined that the initial phase of construction and installation would include only pulsers for the eight waveform components of the first and second types, the trimmer types being deferred. There are now two "reference" designs; one consists of eight of the original twelve components, and the other consists of a re-optimized set of eight components. In conducting this re-optimization a different procedure was used; because no trimmers were assumed to be available, only portions of waveforms away from the bunch ends were fitted well. One can get a better fit, (shown here), even with fewer parameters available, by neglect of the end regions. The two "reference" fits are more fully described, and fitting errors compared, in Table I of Ref. 3.

N	V_{oa}(kV)	V_{ob}	T_{oa}(μs)	T_{ob}	ΔI/I%
1	20	10	-0.4	2.1	0
2	20	4	0.5	2.7	0.8
3	20	3	1.4	3.4	1.5
4	15	8	2.0	3.9	2.2
5	-	-	-	-	2.5

The computer program provides a few measures for evaluating these errors. One is a graph of kinetic energy error (compared with the theoretically desired energy) vs. position along the bunch at the diagnostic gaps $N = 5, 10, 15, \ldots$. (Here only a single graph, at $N = 5$, is used.) From it one may determine the peak-to-peak kinetic energy error excluding the end regions, and also the errors in these regions. The latter might be given little weight at present because the actual bunch shapes at the ends are not known and will probably be uncertain by amounts comparable to the local end-errors observed until the linac comes into operation. An important property of kinetic-energy error is that it can be completely removed (in principle) at any station by applying the proper waveform there; the indicated error includes the effects of waveform errors at all preceding gaps. In contrast, a departure from the desired current variation along the bunch is an integrated effect which develops because velocity errors, as a result of drifting along, lead to downstream accumulated errors in interparticle distances. The computer program provides a diagnostic measure consisting of the percentage variation of current along the bunch at each gap, but excluding the end regions. The quantity presented is $(I_{max}-I_{min})/I_{central}$, denoted above and in the tables of Ref. 3 as $\Delta I/I$; for ideal fitting it would presumably be zero, or nearly so. Values found in the work reported here range up to about 5%.

The effect of changing current from 5 to 2 or 10 mA was evaluated under two assumptions: (1) no changes are made in waveforms, and (2) voltages and on-times of waveform components are re-optimized (again, without trying to fit at bunch ends). With (2) one may fit about as well for each of the three current levels. Details are in Table II of Ref. 3.

The shape parameters chosen are rather arbitrary, and no systematic exploration of the parameter space has been made. However, as an example of sensitivity, comparisons were made between the values 2., 2., and 0.6 μs, for T_I, T_R, and T_I used throughout for the second class and the alternate choice 3., 3., 0.6 μs. The conclusion is that the fitting is not sensitive to this change.

*This acceleration schedule is not unique; in fact, a more ambitious one with greater bunch length compression is under study.

References

1. C.H. Kim and L. Smith, LBL-19137, HI-FAN-272, August 1985.
2. L.J. Laslett (with V.O. Brady), (in this report).
3. David L. Judd, HI-FAR Note 31, Aug. 12, 1985.

REVIEW OF MECHANICAL TOLERANCES FOR MBE-4 ASSEMBLY

David L. Judd

About a year ago several estimates of different types were made on the mechanical accuracy required in assembling the focusing system components of the MBE-16 accelerator then under study. Of these the most sophisticated was a random-error analysis by Lloyd Smith (HI-FAN-251). From this work it appeared that for uniformly distributed errors a maximum error of 2.5×10^{-3} inch (and a related angular error) is allowable if each of three separate effects were to contribute no more than a millimeter to a quadrature sum, for the 30-meter 50-cell MBE-16 system.

Early in August 1985 it appeared that the tolerance requirements for the present MBE-4 system should be reviewed. Assembly work on the first five cells (Section A) had shown that errors in locating the individual rods (in x and y) on plates (containing five, or four, rods each) could be pushed down to the level of ~ 1×10^{-3} inch, but only by use of non-automated techniques to correct occasional assembly errors of order 5×10^{-3} inch of unknown origin. The question thus arose whether or not these larger occasional errors were tolerable in the shorter (15 m) simpler (30-cell) MBE-4 system. In addition, this assembly work provided data on the distribution and size of other tolerances actually achieved.

Smith's analysis leads to evaluation of mean-square coherent beam amplitude $\overline{A^2}$ at the Nth cell in terms of mean squares of three types of randomly-distributed assembly errors. These are:

Δ = transverse displacement of a quadrupole singlet's electrical axis relative to a package,

δ = transverse displacement of a package,

α = rotation of a package.

A package is an assembly of doublets constituting one cell for all the beams (four beams for MBE-4). The value of $\overline{A^2}$ depends on the phase advance σ_0 per cell and the occupancy fraction η; it is proportional (for constant cell length) to the sum

$$N^{-1} \sum_{n=1}^{N} (v_n/v_N)$$

with v_n the ion velocity at the nth cell. Although the value of this sum depends on the specific acceleration schedule in use, and will vary from bunch head to tail, it is rather insensitive: the value ~0.8 is an adequate approximation[1] for MBE-4. Using $\eta = 1/2$, $\sigma_0 \sim 60°$ in Smith's equation leads to

$$\overline{A^2} \simeq \frac{N}{30}\left[(24)^2\,\overline{\Delta^2} + (17)^2\,\overline{(\alpha L)^2} + (11)^2\,\overline{\delta^2}\right],$$

with

L = cell half-length ≃9 inch.

From an Engineering Note by T. Henderson and J. Meneghetti[2] one may estimate $(\alpha L)_{rms}$ and δ_{rms} for assembly of the first five packages into a single unit:

$$(\alpha L)_{RMS} \sim 1.8\times10^{-3} \text{ inch},$$

$$\delta_{RMS} \sim 1.4\times10^{-3} \text{ inch}.$$

These effects contribute ~0.8 mm and ~0.4 mm, respectively, to the quadrature sum. Therefore (as already known in 1984) the effects contributing to Δ_{rms} are the most critical; at the level of 2×10^{-3} inch they contribute ~1.2 mm to the sum.

Contributions to Δ arise not only from errors in positioning individual electrode rods on their plates but also from errors in joining the plates to make a set of singlets and in positioning a singlet set in a package. The latter operations are of a character similar to those contributing to δ, while moving a single rod moves the electrical center roughly half as much. Taking these effects into account, the value $\Delta_{rms} \sim 2\times10^{-3}$ inch represents fairly the results of the procedure used in assembly thus far.

Because beam amplitude A_{rms} increases (for random errors) as $N^{1/2}$, we consider its value at the last cell, N = 30. However, it must be remembered that the linac will be assembled by sections with measurements made at each stage. Should a statistically improbable displacement of unacceptable size occur at an intermediate stage, remedial actions are possible; this feature introduces an element of conservatism, helping to justify comparison of A_{rms} (rather than a multiple of it) with available aperture. Further, it appears that measured assembly errors tend to have a distribution flatter than Gaussian (absence of "points in the tail of the curve"), contributing an additional degree of conservatism.

The physical radius available to a beam is 27 mm, but it appears from simulation calculations[3] that the effects of image charge and higher-order multipole fields may reduce the effective aperture by ~20%, to ~21 mm. The maximum beam radius is estimated to be ~11 mm for 5 mA current; the radial space available to accommodate beam wandering is then ~10 mm, much larger than expected with the rms errors assumed above. Even for $\Delta_{rms} \sim 5\times10^{-3}$ inch the space available is ~three times A_{rms}.

However, the highest-current beams presently contemplated (~13 mA) are larger, roughly $(13/5)^{1/2}(11) \sim 18$ mm, so that for them the errors assumed above are probably acceptable, but are no longer conservatively small.

During the re-examination of this matter, a re-evaluation of the assembly techniques used on Section A led to the conclusion[4] that they could be continued without imposing unacceptable added costs or delays. Therefore the original question about acceptability of occasional 5-mil errors has become moot.

This does not mean that all tolerance questions are resolved. Close monitoring of assembly work will continue; in addition, the program of simulation calculations is not complete.

References

1. Acceleration schedule calculated by C. Kim, evaluated at Bunch center.

2. T. Henderson and J. Meneghetti, "Accelerator Section A - Assembly Measurements," LBL Engineering Note, Code HF3408, Serial M6404, 19 Aug. 1985.

3. C. Celata, informal communications, and work in progress.

4. T. Henderson, informal communication.

Andris Faltens and Arthur Sato

During this period work continued on characterizing the electrostatic energy analyzer and the beam emerging from the SBTE. What had initially appeared to be noisy signals on the wires used to pick up the beam current turned out to be a pair of high frequency oscillations in the beam energy, one at about 8.5 MHz and the other at 1.5 MHz. The amplitude of the oscillations was in the 1% range, while the desired resolution was 0.1%, therefore the first task was to identify the source of the oscillations and eliminate them. The oscillations appeared to be initiated by the turn-on of the source Marx generator, and were successfully eliminated by adding further damping to the Marx column and output capacity. At this point the resolution was measured as 0.4%. To improve the resolution the entrance and exit ports were made more symmetrical and the vertical height of the beamlet striking the detector was decreased from 1 inch to 0.25 inches. After further measurements of the beam, the height was increased to 0.5 inches and the detector wire diameter was increased to 0.020", at which point the signal is near the maximum strength without a significant decrease in the intrinsic resolution. This resulting resolution then was carefully measured and found to be better than 0.3%.[1]

Among the interesting questions related to the SBTE beam and the new analyzer was how well it could measure the longitudinal phase space of the beam, especially at the bunch ends where the most interesting phenomena occur, at high and low intensities. These results are shown in Fig. 1. At the full 12 mA beam current and a slow gun voltage risetime, the beam at the exit of the machine shows a region near the bunch front where the energy is multivalued, essentially a cresting where the faster particles overtake the slower ones. At low intensity, for the same starting energy distribution, the energy is again multivalued, showing a simple shear as the fast body of the bunch passes through the slower particles which were initially at the front of the bunch. At both of these intensities the actual measurements in the analyzer were done with a few microamperes of current at the detector, read directly on a 120 ohm termination at an oscilloscope.

At the time the measurements were made there was an unreproducibility in the beam energy which was several times larger than could be accounted for by fluctuations in either the source or spectrometer voltages. Because only two spectrometer wires were observed simultaneously on a fast time scale, the experimental points shown in Fig. 1 indicate the range of energies observed in different pulses at corresponding times within the pulse, and the minimum (line through black dots) and maximum (line through squares) times observed on one pulse at the given energy. An eventual goal in the program is to be able to simultaneously read all of the detectors and to display the data in a processed form, using fast sample-and-hold circuitry. At this time the results were assembled from many pulses over a period of hours, during which time the energy window of two wires in the detector was moved through the range of interest.

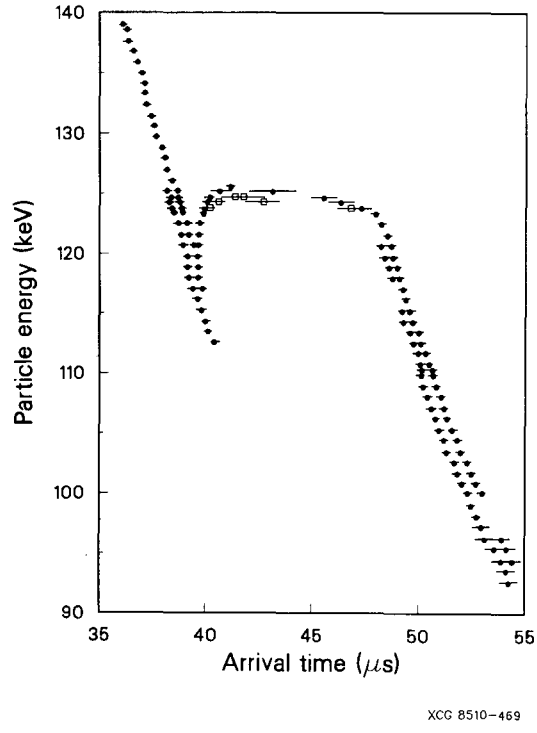

Fig. 1a. Full beam energy vs. time at Deep Faraday Cup after Q82

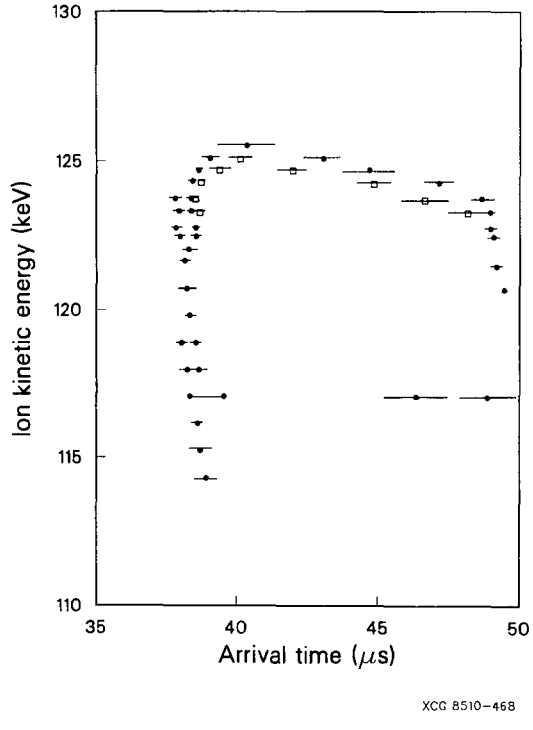

Fig. 1b. Energy spectrum of the 3 1/2% intensity beam at the exit of the transport line after Q82

References

1. An Electrostatic Energy Analyzer for Longitudinal Energy Measurements, A.H. Sato, HIFAN-296.

A FAST SIMPLE DETECTOR FOR THE HIFAR ENERGY ANALYZER

T. J. Fessenden

During this last period a detection method for determining the energy of ions entering the HIFAR ion energy analyzer[1] was developed which determines the mean energy of the beam as a function of time at the plane of the detector. The advantage of this detection method is that fast measurements of the average energy of the beam are quickly and easily performed. A disadvantage is that the method does not detect two or more distinct beams simultaneously striking the detector.

The Ion Energy Analyzer and Detector

The energy analyzer was described in the last HIFAR Semi-annual Report by Rosenblum and Faltens.[1] The cesium beam is apertured at the entrance to the analyzer by one of three slits that are 20, 40, and 80 thousandths of an inch wide. The resulting ribbon beam travels through the analyzer and is refocussed to the same width by the analyzer fields at the plane of the detector as is described in Ref. 1.

The detector is an array of thirty 0.02 inch wires located 0.031 inches apart. Thus the total width of the detector (L) is 0.92 inches. The narrowest beam is about equal to the space between the wires. The broadest beam spans approximately 2.5 wires. The detector is wired as shown schematically in Fig. 1. R_1 and R_2 are 150-ohm resistors in parallel with the 50-ohm cable terminating resistors. The individual detector wires are connected by 29, ten-ohm resistors as shown.

The voltages V_1 and V_2 are related to the mean beam position on the detector array $\langle x\rangle$ by

$$\langle x\rangle/L = (0.5+R_1/nR)(V_2-V_1)/(V_2+V_1) \qquad (1)$$

where $\langle x\rangle$ is defined by

$$\langle x\rangle/L = x_n i_n/I \ . \qquad (2)$$

Here i is the current striking the nth wire located x_n from the center of the array of length L, and I is the total current striking the array. Thus the output voltages V_1 and V_2 respond to the weighted average of the energy of the beam striking the detector.

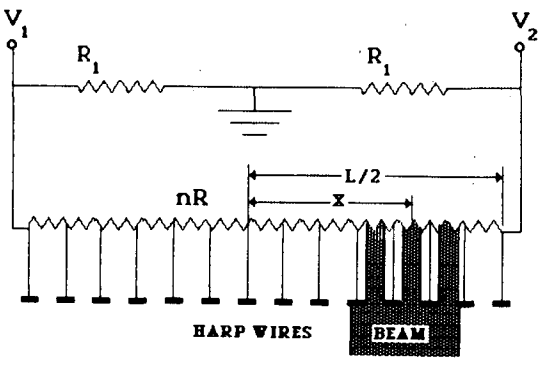

XBL 8510-4264

Fig. 1. Schematic of the Detector Circuit

For the parameters used in the experiments and shown in Fig. 1, $\langle x\rangle/L$ is given by

$$\langle x\rangle/L = 0.629\ (V_2-V_1)/(V_2+V_1) \qquad (3)$$

This expression does not depend on the beam current except that voltages V_1 and V_2 will both be zero if the current is zero. The sum of these voltages measures the beam current striking the detector according to

$$I = (V_1+V_2)/R_1 \ . \qquad (4)$$

The energy of the beam that follows the central ray and strikes the center of the detector is given by:

$$E_o = R_c V_d/2d \ . \qquad (5)$$

Here R_c is the radius of curvature of the analyzer (18 in), V is the voltage between the analyzer plates and d is the spacing between the plates (1 in). The mean energy of the beam $\langle E\rangle$ is then given by

$$\langle E\rangle = E_o(1+\langle x\rangle/R_c) \qquad (6)$$

An illustration of this method of using the energy analyzer is contained in the note by A.I. Warwick[2] in this report.

Energy Measurements Using Zero Crossings

A second method of obtaining energy measurements is to vary the voltage applied to the deflection plates (V_d) and observe the instants of time at which V_2-V_1 equals zero. Figure 2 illustrates measurements of the energy of the beam on SBTE using this technique. The oscillogram shows three detector outputs at voltages of + or - 6.764 kV, 6.835 kV, and 6.876 kV from each deflection plate ground. By varying the deflection voltage and observing the time of the trace zero crossings the time dependence of the energy of the SBTE beam shown in Fig. 3 was obtained. This technique has two advantages. It only requires an oscilloscope that can form V_2-V_1 as a function of time.

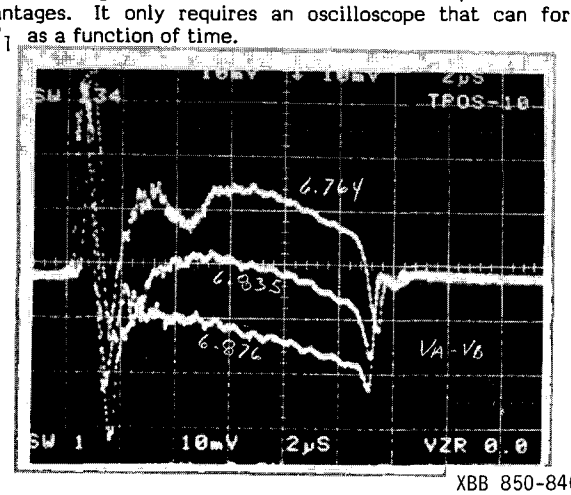

XBB 850-8405

Fig. 2. Oscillograms of the Energy of the SBTE Beam versus Time

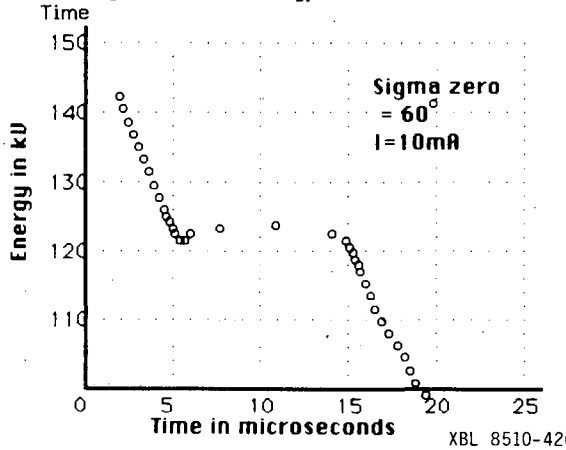

XBL 8510-4263

Fig. 3. Measurement of the Energy of the SBTE Beam Versus Time

References

(1) S. S. Rosenblum and A. Faltens, Electrostatic Energy Analyzer, in HIF Half Year Report, LBL-19501, p. 9 (1985).

(2) A. Warwick, Current and Kinetic Energy Waveforms from the MBE-4 Injector, this report.

HI-FAN Notes

HI-FAN-273 LBL-19601	D. Keefe	Developments in Accelerators for Heavy Ion Fusion IEEE Trans. on Nucl. Sci., 32, No. 5, 3277 (Oct. 1985)
HI-FAN-274 LBL-19487	A.I. Warwick	Alumino-Silicate Ion Sources for Accelerator Applications IEEE Trans. on Nucl. Sci., 32, No. 5, 1809 (Oct. 1985)
HI-FAN-275 LBL-19560	E.P. Lee T.J. Fessenden	Transportable Charge in a Periodic Alternate Gradient System IEEE Trans. on Nucl. Sci., 32, No. 5, 2489 (Oct. 1985)
HI-FAN-276 LBL-19526	A. Faltens S. Rosenblum	Investigation of Re-X Glass Ceramic for Accelerator Insulating Columns IEEE Trans. on Nucl. Sci., 32, No. 5, 3131 (Oct. 1985)
HI-FAN-277 LBL-19602	E.P. Lee	The High Temperature Experiment; Choice of Parameters IEEE Trans. on Nucl. Sci., 32, No. 5, 3335 (Oct. 1985)
HI-FAN-278 LBL-19647	M.G. Tiefenback D. Keefe	Measurements of Stability Limits for a Space-Charge-Dominated Ion Beam in a Long A.G. Transport Channel IEEE Trans. on Nucl. Sci., 32, No. 5, 2483 (Oct. 1985)
HI-FAN-279 LBL-19485	C.M. Celata I. Haber L.J. Laslett L. Smith M.G. Tiefenback	The Effect of Induced Charge at Boundaries on Transverse Dynamics of a Space-Charge-Dominated Beam IEEE Trans. on Nucl. Sci., 32, No. 5 2480 (Oct. 1985)

HI-FAN-280 LBL-19620	R.T. Avery C.S. Chavis T.J. Fessenden D.E. Gough T.F. Henderson D. Keefe J.R. Meneghetti C.D. Pike D.L. Vanecek A. Warwick	MBE-4, A Heavy Ion Multiple-Beam Experiment IEEE Trans. on Nucl. Sci., 32, No. 5 3187 (Oct. 1985)
HI-FAN-281 LBL-19563	C. Kim V.O. Brady T.J. Fessenden L.J. Laslett D. Judd L. Smith	Synthesis of MBE-4 Accelerating Waveforms IEEE Trans. on Nucl. Sci., 32, No. 5 3190 (Oct. 1985)
HI-FAN-282 LBL-19484	A. I. Warwick D. Vanecek O. Fredriksson	A Four-Beam Cesium Injector for MBE-4 IEEE Trans. on Nucl. Sci., 32, No. 5 3196 (Oct. 1985)
HI-FAN-283 LBL-19527	C.M. Celata V. Brady I. Haber L.J. Laslett L. Smith	The Effect of Focusing Field Nonlinearities in MBE-4 on Transverse Beam Dynamics IEEE Trans. on Nucl. Sci., 32, No. 5 3193 (Oct. 1985)
HI-FAN-284 LBL-19529	G.A. Krafft C.H. Kim L. Smith	The LBL Neutralized Beam Focusing Experiment IEEE Trans. on Nucl. Sci., 32, No. 5, 2486 (Oct. 1985)
HI-FAN-285 LBL-19501	H.I.F. Staff	Heavy Ion Fusion Half Year Report October 1, 1984 - March 30, 1985
HI-FAN-286 LBL-18987	L.J. Laslett	Nonlinear Dynamics: A Personal Perspective Presented at the Joint US/CERN School on Particle Accelerators, Sardinia, Italy, Jan. 31 - Feb. 5, 1985
HI-FAN-287	L.J. Laslett	Transportable Current and Lattice Design In an A-G Electrostatic-Quadrupole Transport Lattice. (6/14/85)

HI-FAN-288 LBL-19797	L.J. Laslett	Hamiltonian Systems in Accelerator Physics Proceedings of the Orbital Dynamics Workshop, Lawrence Berkeley Laboratory, Berkeley, CA, March 7-12, 1985; to be published in Particle Accelerators
HI-FAN-289 LBL-19798	Edward P. Lee	Model Equations for High Current Transport Proceedings of the Orbital Dynamics Workshop, Lawrence Berkeley Laboratory, Berkeley, CA, March 7-12, 1985; to be published in Particle Accelerators
HI-FAN-290 LBL-19796	Edward P. Lee J. Hovingh A. Faltens	Heavy-Ion Fusion System Assessment Project Quarterly Status Report, Jan.-Mar. 1985 (6/85)
HI-FAN-291	R. Dormido W.G. Ghiorso L. Schalz S.S. Rosenblum	An Automated System for Measuring Vacuum Outgassing Rates. (8/85)
HI-FAN-292	J. Bisognano E. P. Lee	Numerical Studies of High Current Beam Compression in Heavy Ion Fusion. (7/85)
HI-FAN-293 LBL-19809	Charles Kim	High Current Beam Transport with Multiple Beam Arrays Invited talk given at the Workshop on High Brightness, High Current, High Duty Factor, Ion Injectors, San Diego, Calif., May 21-12, 1985
HI-FAN-294 LBL-19592	R.T. Avery	Program Plan for the MBE-4 Multiple Beam Experiment February 1985. (7/85)
HI-FAN-297	Denis Keefe	Working Group 3: High-Current Beam Transport Invited talk given at the Workshop on High Brightness, High Current, High Duty factor, Ion Injectors, San Diego, Calif., May 21-12, 1985
HI-FAN-298	L. Smith	Chairman's Summary for Working Group on Theory and Simulation for High Current R.F. Accelerators Invited talk given at the Workshop on High Brightness, High Current, High Duty factor, Ion Injectors, San Diego, Calif., May 21-12, 1985

HIFAR Notes (Internal and Informal)

HIFAR Note #1	Tom Fessenden	"Hifar Notes" (10/11/84)
HIFAR Note #2	Tom Fessenden Charles Kim	"SBTE Experiments for the First Half of FY-85" (10/17/84)
HIFAR Note #3	C.H. Kim L. Smith	"Discrete Acceleration and Bunching in an Ion Induction Linac" (10//9/84)
HIFAR Note #4	S. Rosenblum	Excerpt from memo from Faltens and Rosenblum to Fessenden and Chupp (7/9/84)
HIFAR Note #5	Naseem Munshi	Various notes about cast insulators (11/14/84)
HIFAR Note #6	T.J. Fessenden	Lumped Circuit Waveform Synthesis for MBE-4 Phase 1 (11/15/84)
HIFAR Note #7	Jackson Laslett	The Projected H.-T.-E. Revisited (4/84) 11/30/84
HIFAR Note #8	Jackson Laslett	Concerning the Magnetic Focusing Lattice of the H.-T.-E. (4/84) 12/84
HIFAR Note #9	A. Warwick	MBE 4 Injector Development (12/5/84)
HIFAR Note #10	M. Tiefenback	Short Note Concerning E_N vs Z in SBTE (12/84)
HIFAR Note #11	S. Rosenblum A. Faltens	Quad High Voltage Test 01/07/85
HIFAR Note #12	D. Gough	MBE4 Steering (1/85)
HIFAR Note #13	C. Kim	Synthesis fo MBE4 Accelerating Waveforms (1/85)
HIFAR Note #14	B. Avery	MBE-4 Steering Sensitivity Calculation (2/85)
HIFAR Note #15	D. Gough	MBE-4 Pulsers (2/85)
HIFAR Note #16	R. Avery	MBE-4 Location of Diagnostics Devices (3/85)
HIFAR-Note #17	A. Faltens S. Rosenblum	Electrostatic Energy Analyzer (EEA) for HIFAR (2/85)

HIFAR-Note #18	C. Pike	Proposed Energy Analyzer Data Acquisition System (4/85)
HIFAR-Note #19	HIF	Heavy Ion Fusion Accelerator Research
HIFAR-Note #20	T.J. Fessenden	A. Capacitive Beam-Charge Monitor For SBTE (4/85)
HIFAR-Note #21	A. Faltens	Energy and Current Variations (4/85)
HIFAR-Note #22	C. Pike	Preliminary Electrical Data for Castable Epoxy Samples (4/85)
HIFAR-Note #23	C.Kim V. Brady T. Fessenden D. Judd L. Laslett	Reference Longitudinal Physics Design of MBE-4 (4/85)
HIFAR-Note-24	E.C. Hartwig	Pulsed Quadrupoles to Provide Accelerator (5/85) (7/85)
HIFAR-Note-25	L.J. Laslett	Parameters for Matched-Envelope Radii in Symmetric Hard-Edge A-G Quadrupole Lattices (7/85)
HIFAR-Note-26	L.J. Laslett	Runge-Kutta-Gill Integration of Coupled First-Order Ordinary Differential Equations (7/85)
HIFAR-Note-27	L.J. Laslett	Gaussian Integration for $-1 \leq \leq +1$ (7/85)
HIFAR-Note-28	L.J. Laslett	Equivalent Hard-Edge Lattice (7/85)
HIFAR-Note-29	A. Warwick	Measured Current Profiles After Matching in MBE 4
HIFAR-Note-30	D. Brodzik	Pulser Waveforms in MBE-4 (7/85)
HIFAR-Note-31	D. L. Judd	Present Status of Computational Guidelines for Design, Construction, and Installation of Acceleration Hardware in Section A (GAPS 1-4) of ME-4 8/12/85
HIFAR-Note-32	D. Brodzik	Accelerator A - Guidelines (8/85)

HIFAR-Note-33	D. Judd	Present Status of Computational Guidelines for Design, Construction, and Installation of Acceleration Hardware in Section A (GAPS 1-4) of MBE-4 (8/85)
HIFAR-Note-34	T. Henderson	Accelerator Section A - Assembly Measurements (8/85)
HIFAR-Note-35	T. Warwick	Energy and Current Measurements from MBE-4 Injector (8/85)
HIFAR-Note-36	L.J. Laslett V.O. Brady	Waveforms for Longitudinal Dynamics (HIF Semi-Annual Report).
HIFAR-Note-37	David L. Judd	Summary of Discussion on Sept. 10 of Mechanical Tolerances for MBE-4 Assembly.
HIFAR-Note-38	T.J. Fessenden	A Fast Simple Detector for the HIFAR Energy Analyzer 9/23/85
HIFAR-Note-39	A. Faltens	Multiple Pulsing with Existing Technology 10/2/85
HIFAR-Note-40	C. Kim	Trimmer Pulser Wave Forms for MBE-4 Section A (10/15/85)
HIFAR-Note-41	D. Brodzik	Silicon Steel Tests (single core)
HIFAR-Note-42	R. Avery C. Pike	MBE-4 Fabrication Plan for FY86.
HIFAR-Note-43	David L. Judd	Summary of Discussion on Sept. 10 of Mechanical Tolerances for MBE-4 Assembly

H.I.F. STAFF ROSTER

Denis Keefe

Robert T. Avery
Donald A. Brodzik
Clarence Chavis
Warren Chupp
Andris Faltens
Thomas J. Fessenden
David Gough
Edward C. Hartwig
T. Henderson
Ralph Hipple
Charles H. Kim
John Meneghetti
Chester D. Pike
Gerald L. Stoker
Michael Tiefenback
David Vanecek
Anthony Warwick

Lloyd Smith

Victor Brady
Christine Celata
David L. Judd
Geoffrey Krafft
L. Jackson Laslett
Edward P. Lee

William B. Herrmannsfeldt, SLAC

H.I.F. END OF THE YEAR REPORT: DISTRIBUTION LIST

Allied Chemical Corporation

Carl Smith

Argonne National Lab.

Frank T. Cole
Thomas A. Fields
Ronald Martin

University of Arizona

R. Morse

Batelle

John Hartman

Bechtel

W. Allen

BMD/ATC

Milton Hawie

Brookhaven National Lab.

Mark Barton
E. Courant

C.E.A. Bruyeres-le-Chatel

R. Dei-Cas

CEBAF

J. Bisognano
D. Douglas
H. Grunder
C. Leemann

University of Calif., Irvine

Norman Rostoker

Cornell University

John Nation
Ravi N. Sudan

DARPA

Joseph Mangano

Department of Defense (SDIO)

Richard Gullickson
Gerold Yonas

Department of Energy

DP-OIF

Sheldon L. Kahalas
L. Killion
R. Schriever
Marshall Sluyter
Col. Charles Whited

ER

Rysgard Gajewski (AEP)
Terry Godlove (HENP)
Gerry Peters (HENP)
Robert Rader (OPA)
D. Stevens (BES)
David F. Sutter (HENP)
Alvin Trivelpiece, Dir.,
Office of Energy Research
William Wallenmeyer (HENP)

DoE San Office

Rudolf Bredderman
Dennis Neely

E.P.R.I.

Robert Scott

Fermi National Accelerator Lab.

Fred Mills
Lee Teng

F.O.M. Amsterdam

F. Siebenlist

GANIL

P. Lapostolle

GE

John Lucek

GSI

R. Bock
D. Boehne
I. Hofmann

University of Illinois

G. Miley

Institute for Nuclear Study

Y. Hirao

KMS Fusion, Inc.

Alex Glass
Michael J. Monsler

Kanazawa University

S. Kawasaki

Lawrence Berkeley Laboratory

D. Atwood, 80/101
R. Avery, 46/189
K. Berkner, 50/149
D. Brodzik, 46/125
C. Celata, 47/112
W.W. Chupp, 47/112
M. Cornacchia, 47/112
T. Elioff, 90/4040
A. Faltens, 47/112
T. Fessenden, 47/112
A. Garren, 47/112
D. Gough, 47/112
E. Hartwig, 47/112
H. Heckman, 50/245
T. Henderson, 46/161
E. Hoyer, 46/187
E. Hyde, 50A/4133E
R. Johnson, 50A/4119
D. Judd, 47/112
D. Keefe, 47/112
C. Kim, 47/112
G. Krafft, 47/112
M. Krebs, 50A/4112
W. Kunkel, 4/230
G. Lambertson, 47/112
L.J. Laslett, 47/112
E.P. Lee, 47/112
E. Lofgren, 47/112
J. Marx, 50/149
J. Meneghetti, 46/161
J. Peterson, 90/4040
A. Sessler, 4/230
D. Shirley, 50A/4133
L. Smith, 47/112
C. Taylor, 46/161
M. Tiefenback, 47/112
D. Vaughan, 50/149
D. Vanecek, 58/1011
A.I. Warwick 47/112

Lawrence Livermore Laboratory

Roger Bangerter, L-477
W. Barletta, L-626
Richard J. Briggs, L-321
John L. Emmett, L-488
Darwin Ho, L-477
John Holzrichter, L-481
William Krupke, L-488
J. Lindl, L-477
Jim Mark, L-477

Lawrence Livermore Laboratory (cont'd)

John Nuckolls, L-477
Louis Reginato, L-526
Erik Storm, L-481

Lockheed

John Siambis

Los Alamos National Laboratory

Ihor Bohachevsky
Richard Cooper
Robert Jameson
Earl Meyer
Roger B. Perkins
Steve Rockwood
Richard Stokes
Tai-Sen Wang
Doug Wilson

University of Maryland

Martin Reiser
Derek Tidman

Max Planck Inst. fur Plasma Physik Garching

Arnulf Schluter

Maxwell Laboratories

Library

National Bureau of Standards

S. Penner
M. Wilson

Naval Research Lab.

Steven Bodner
T. Coffey
Irving Haber
Philip Sprangle
Peter Turchi

Occidental Research Corp.

Wyn Salisbury

Osaka University

T. Mochizuki
C. Yamanaka

Universita di Padova

A. Pascolini
M. Pusterla

Physical Dynamics

G. H. Gillespie

Physics International

Library

Pulse Sciences, Inc.

Ian Smith
Kurt Nielson

RAFAEL

Joseph Shiloh

Rutherford Laboratory

John D. Lawson
Chris Pryor

Sandia Laboratories

Everet H. Beckner
Don Cook
Glenn Kuswa
Tom Martin
J.P. Vandevender

SLAC

William Herrmannsfeldt, Bin 26
Burton Richter, Bin 7

Soka University

Tetsuya Saito

SOREQ Nuclear Research Center

A. Sternlieb

TRW

J. Gordon
Z. Guiragossian
J. Maniscalco
A.W. Maschke
W. Steele

UCLA

John Dawson

University of Texas at Austin

Toshi Tajima

URA

Edward Knapp

Varian

S.S. Rosenblum

Westinghouse

M. Nahemow
E. W. Sucov

University of Wisconsin

G. Kulcinski
G. Moses
R. Peterson

This report was done with support from the Department of Energy. Any conclusions or opinions expressed in this report represent solely those of the author(s) and not necessarily those of The Regents of the University of California, the Lawrence Berkeley Laboratory or the Department of Energy.

Reference to a company or product name does not imply approval or recommendation of the product by the University of California or the U.S. Department of Energy to the exclusion of others that may be suitable.

LAWRENCE BERKELEY LABORATORY
TECHNICAL INFORMATION DEPARTMENT
UNIVERSITY OF CALIFORNIA
BERKELEY, CALIFORNIA 94720